

DEVELOPMENT AND CHARACTERIZATION OF
ENVIRONMENTALLY BENIGN,
CORROSION-INHIBITING,
DRY FILM LUBRICANT
COATINGS

Presented to the Graduate Council
of Texas State University – San Marcos
in Partial Fulfillment
of the Requirements

for the Degree
Master of Science
by

Aureliano Perez, Jr.

San Marcos, Texas
December 2005

ACKNOWLEDGEMENTS

As I begin, I wish to thank the members of my graduate committee:

Dr. Patrick E. Cassidy, Dr. John Massingill and Dr. George P. Hansen. I express my utmost appreciation to Dr. Cassidy for his patience, guidance and interest throughout the completion of this work. I consider myself fortunate to have been given the opportunity to work with such an insightful educator and scientist. I would also like to convey my gratitude to Dr. Hansen who continues to be a wonderful and inspirational mentor, colleague and friend.

I offer my appreciation to my employer, Dr. J. Scott Thornton, who afforded both the foundation and the opportunity for me to conduct this research. In addition, I wish to thank my colleagues and friends at Texas Research Institute, especially John Bulluck, who offered support and encouragement in the practical development and characterization of the material upon which this study is based.

I offer my thanks to my parents, Aureliano Sr. and Theresa, for their love, understanding, hard work, sacrifices and perseverance in providing me the opportunities of a university education.

I would finally like to thank Charlotte, who is my best friend and wife. I will be forever grateful to her for the many gifts of life and love that she shares with me.

This manuscript was submitted on November 21, 2005.

TABLE OF CONTENTS

	Page
ACKNOWLEDGEMENTS.....	iii
LIST OF TABLES.....	vi
LIST OF FIGURES.....	viii
ABSTRACT.....	xi
CHAPTER 1 INTRODUCTION.....	1
1.1 Motivation.....	1
1.2 Objectives.....	1
1.3 Overview of Thesis.....	2
CHAPTER 2 BACKGROUND.....	3
2.1 Tribology.....	3
2.2 Friction and Wear.....	4
2.3 Lubricants.....	5
2.4 Dry Film Lubricants.....	5
2.5 Molybdenum Disulfide.....	7
2.6 Binder Resin Systems.....	8
2.7 Waterborne Polyurethane Dispersions.....	9
2.8 Coalescence.....	11
2.9 Falex Pin and Vee Block Tester.....	12
2.10 Corrosion Control.....	14
2.11 Design of Experiments.....	17
2.12 Characterization.....	18
CHAPTER 3 EXPERIMENTAL.....	19
3.1 MIL-L-23398 Solid Film Lubricant Performance Specification.....	19
3.2 Silicate Based Lubricants.....	21
3.3 Polyurethane Dispersions	22
3.4 Load Carrying Capacity.....	28

3.5	Endurance Life and Temperature Effects.....	29
3.6	Corrosion Control.....	30
3.7	Adhesion and Chemical Resistance.....	43
3.8	Thermal Shock Sensitivity.....	46
3.9	Aluminum Corrosion Resistance.....	47
3.10	Sulfurous Acid Salt Spray.....	47
3.11	Storage Stability.....	48
CHAPTER 4 DESIGN OF EXPERIMENTS.....		49
4.1	Designation of Factors.....	49
4.2	Designation of Responses.....	50
4.3	Optimization.....	56
CHAPTER 5 SPECTROSCOPIC ANALYSIS OF THE DRY FILM LUBRICANT...58		
5.1	Optical Microscopy.....	58
5.2	X-ray Photoelectron Spectroscopy.....	61
5.3	Atomic Force Microscopy.....	73
5.4	Fourier Transform Infrared Analysis.....	81
CHAPTER 6 CONCLUSIONS.....		87
6.1	Endurance Life and Corrosion Resistance.....	87
6.2	Characterization.....	88
6.3	Future Work.....	91
REFERENCES.....		93

LIST OF TABLES

	Page
Table 3.1	MIL-L-23398D performance requirements.....20
Table 3.2	Endurance Life and Load-Carrying Capacity of Silicate-Based Solid Film Lubricants.....22
Table 3.3	Materials for urethane dispersion-based formulations.....23
Table 3.4	Endurance life comparisons of urethane <i>versus</i> silicate based lubricants.....25
Table 3.5	Endurance life performance of commercial lubricants.....26
Table 3.6	Compositions, parameters and performance of seven key formulations27
Table 3.7	Summary of corrosion control additives formulated into the lubricant.....34
Table 3.8	Summary of surfactant additives formulated into the lubricant.....35
Table 3.9	Urethane resin analysis and results38
Table 3.10	Corrosion performance as a function of solids content38
Table 3.11	Corrosion resistance as a function of coalescent blend.....39
Table 3.12	Tabulated results of final formula optimization42
Table 4.1	Optimal mixture design over three factors.....50
Table 4.2.	Analysis of four replicate pairs from the mixture design.....52

Table 5.1	Analytical conditions of the XPS experiments.....	62
Table 5.2	Concentration of Elements at the SURFACE from XPS Medium Resolution Data.....	72
Table 5.3	AFM roughness results.....	79
Table 5.4	Description and explanation of the Image Statistics.....	79

LIST OF FIGURES

	Page
Figure 2.1	Lamellar structure of graphite7
Figure 2.2	Lamellar structure of molysulfide.....8
Figure 2.3	Diagram of Falex pin and vee block set.....12
Figure 2.4	The Falex pin and vee block tester.....13
Figure 2.5	Components of an electrochemical cell.....15
Figure 2.6	A metal surface as a component of an electrochemical cell.....16
Figure 3.1	Load carrying capacity performance of lubricant A2200-91.....28
Figure 3.2	A digital pyrometer with laser.....29
Figure 3.3	Temperature and torque measurements during endurance life test.....30
Figure 3.4	Salt fog chamber31
Figure 3.5	Coated metal panels after salt fog exposure.....32
Figure 3.6	Corroded panel after salt fog exposure.....33
Figure 3.7	Corroded panel with lubricant containing inhibitors.....33
Figure 3.8	Corroded panels with lubricant containing surfactants.....36
Figure 3.9	Steel panels coated with various resins37
Figure 3.10	Steel panel coated with corrosion resistant lubricant.....40

Figure 3.11	Steel panel coated with a urethane/acrylic resin blend.....	41
Figure 3.12	Adhesion test procedures.....	43
Figure 3.13	Coated panels immersed in aggressive fluids.....	44
Figure 3.14	Coated panel after immersion in gun cleaning fluid.....	45
Figure 3.15	Coated panel after immersion in jet fuel	45
Figure 3.16	Laboratory arrangement for thermal shock treatment.....	46
Figure 3.17	Coated panels after thermal shock	47
Figure 4.1	Plot of endurance life <i>versus</i> MoS ₂ concentration.....	53
Figure 4.2	Plot of corrosion <i>versus</i> resin content.....	53
Figure 4.3	Response surface contour diagram of endurance life over three factors...54	
Figure 4.4	Response surface contour diagram of corrosion over three factors	56
Figure 4.5	Optimization contour diagram	57
Figure 5.1	Optical microscopy of unworn test standard and specimen after mild wear.....	59
Figure 5.2	Digital image of lubricant surface defect	59
Figure 5.3	Surface topography after 30-minutes of extreme pressure wear.....	60
Figure 5.4	Digital image of lubricant failure.....	60
Figure 5.5	Survey spectra of unworn and pristine specimens.....	64
Figure 5.6	Survey spectra of specimen subjected to break-in load.....	64
Figure 5.7	Survey spectra of specimen taken mid point of endurance life.....	65
Figure 5.8	Survey spectra of specimen taken at lubricant failure.....	65
Figure 5.9	Medium resolution spectra of unworn test standard.....	66
Figure 5.10	Medium resolution spectra of specimen 2	67
Figure 5.11	Medium resolution spectra of specimen 3.....	68

Figure 5.12	Medium resolution spectra of specimen 4.....	69
Figure 5.13	Components of the AFM spectrometer	73
Figure 5.14	AFM roughness analysis of Specimen 1.....	75
Figure 5.15	AFM 3-dimensional view of Specimen 1.....	75
Figure 5.16	AFM roughness analysis of Specimen 2.....	76
Figure 5.17	AFM 3-dimension view of Specimen 2.....	76
Figure 5.18	AFM roughness analysis of Specimen 3.....	77
Figure 5.19	AFM 3-dimension view of Specimen 3.....	77
Figure 5.20	AFM roughness analysis of Specimen 4.....	78
Figure 5.21	AFM 3-dimension view of Specimen 4.....	78
Figure 5.22	FT-IR spectrum of Specimen 1.....	82
Figure 5.23	Reference spectra of neat poly(tetrafluoroethylene).....	83
Figure 5.24	FT-IR spectrum of Specimen 2.....	84
Figure 5.25	FT-IR spectrum of Specimen 3.....	85
Figure 5.26	Figure 5.22 FT-IR spectrum of Specimen 3.....	86

ABSTRACT

DEVELOPMENT AND CHARACTERIZATION OF
ENVIRONMENTALLY BENIGN,
CORROSION-INHIBITING,
DRY FILM LUBRICANT
COATING

by

Aureliano Perez, Jr., B.S.

Texas State University – San Marcos

December, 2005

SUPERVISING PROFESSOR: PATRICK E. CASSIDY

Solid film lubricants have found highly specialized utility in demanding, extreme-pressure tribology applications where conventional oils and greases cannot be employed. Early examples of dry film lubricants (DFL) contained toxic materials such as lead, antimony oxide and arsenic, as well as flammable, ozone-depleting solvents with

suspected carcinogenic activity. The best performing lubricants still in use today continue to employ these noxious components. Graphite is also prevalent in many conventional solid film lubricants. Unfortunately graphite promotes galvanic corrosion, particularly on steel substrates where these lubricants are widely utilized. Few changes have been made to early dry film lubricant formulations that are used in modern applications. However, on-going promulgation of strict environmental and safety regulations has severely restricted further use and development of solid film lubricants based on miasmatic chemistries.

The goal of this work was to develop and characterize a solid film lubricant coating that does not contain volatile organic solvents, is free of human and environmental toxins, provides exceptional corrosion protection and cures at ambient temperature. It was to provide equal or improved endurance and lubricating properties as the nearly defunct chemistries from previous generations. The solid film lubricant coating developed in this study was tested to meet all performance requirements in Military Specification MIL-L-23398. An optimized combination of waterborne polyurethane resin, molybdenum disulfide, polytetrafluoroethylene, and coating additives produced a lubricant that met all requirements. Falex Pin and Vee Block testing for endurance life and load carrying capacity were extensively used to determine tribological performance. X-ray photoelectron spectroscopy, atomic force microscopy, optical microscopy and Fourier transform infrared analysis were employed to characterize underlying physical and chemical mechanisms of wear subjected to the lubricant. XPS and FTIR analysis showed dynamic reactions occurred on the surface of the lubricant

during wear. Molybdenum oxidized under extreme pressure loads and sulfide changed to sulfate.

CHAPTER 1

INTRODUCTION

1.1 Motivation

The United States Naval Air Systems Command (NAVAIR) enlisted the assistance of a private, contract research firm to develop and characterize a dry film lubricant coating that is free of toxic components and volatile organic compounds (VOC), capable of sustaining extreme pressure loads, and able to provide corrosion protection to metallic substrates. The author was selected to conduct this study while obtaining his Master of Science degree.

NAVAIR and other interested agencies within the DOD must also comply with emerging environmental and occupational exposure guidelines. Heritage DFL coatings pre-date and fail recently mandated requirements and are soon to be restricted from further use. It is imperative that alternative products based upon state of the art, environmentally acceptable technologies be developed as suitable replacements.

1.2 Objectives

The goal of this work was to develop a low volatile organic content (VOC) solid film lubricant. This thesis also endeavored to characterize the new DFL product using

spectroscopic techniques. Characterization will aid in the understanding of physical and chemical changes of lubricants under extreme pressure conditions.

1.3 Overview of Thesis

Dry film lubricant technologies and fundamental concepts of tribology are described in Chapter Two. Also presented are fundamental concepts of coatings and corrosion control. Experimental testing procedures and key aspects of military specification MIL-L-23398 that governed development of the product will be presented in Chapter Three. Chapter Four presents an experimental design that was conducted to efficiently evaluate key parameters used to refine the lubricant composition. Chapter Five includes spectroscopic experiments conducted to characterize the product. Analysis of results from the tests described in Chapter Three and Chapter Five are presented in Chapter Six. Conclusions drawn from this study and recommendations for further research are also presented in Chapter Six

CHAPTER 2

BACKGROUND

2.1 Tribology

Tribology encompasses the study of lubrication. The word originates from the Greek *tribos*, which means rubbing. Tribology is the science of interacting surfaces in relative motion and focuses on friction, wear, lubrication and contact mechanics. Four major scientific fields independently conduct research in the field of tribology.²⁸ These are solid mechanics (mathematics of contact stresses and surface temperatures due to sliding), fluid mechanics (mathematics of liquid lubricant behavior), material science (atomic and microscale mechanisms of solid surface degradation) and chemistry (orderly chemical alteration of bulk lubricants and testing of lubricants). A paucity of work on chemical-physical processes in the contacting and sliding region has been noted.²⁹ Those who undertake the challenges of tribology will undoubtedly encounter the subject in materials science, fluid dynamics, chemistry, physics, heat transfer and surface characterization, among others. These are tools used by tribologists to design materials with improved wear resistance, reduced friction and survivability in extreme conditions.

2.2 Friction and Wear

Friction and wear are detrimental to machines, with consequences of reduced performance, increased energy consumption and cost. Piston rings of a combustion engine are designed to operate efficiently when the surface of the ring and bore are smooth. When frictional forces between the ring and bore are minimal, greater engine efficiency is achieved. Poor lubrication from contaminated oil increases frictional forces, with consequences that include increased fuel consumption, pronounced reduction in performance and premature engine wear.

The onset of wear is a consequence of friction and occurs when a mass or volume of material is removed from a surface that is repeatedly stressed in mechanical contact with another body. The loss leads to increased clearances between moving components. Wear of mechanical components is divided into two separate categories. First is adhesive wear, which occurs when a component moves over another component and contact is made between the peaks of surface roughness. These asperities adhere together and form localized welds, while particulates from softer asperities shear off and adhere to the harder surface. The particles become dislodged through continuous motion and become abrasive. This leads to the second wear category known as abrasive wear. Damage caused by abrasive wear of a machine component occurs when hard particles are forced against and slide across its surface. Wear in any form can lead to mechanical failures with consequences that range from arbitrary to catastrophic. Designers and engineers develop machines and parts with finite and predictable working lifetimes. However, unforeseen or unanticipated wear can rapidly accelerate the premature breakdown of a mechanical part. If that part happens to be the spring mechanism of a small mousetrap

the consequences are minor but irritating. However, if the part is the thrust bearing of an aircraft engine, the consequences are catastrophic.

2.3 Lubricants

Lubricants are available in several forms and are formulated for specific applications. The primary function of a lubricant is to separate contacting surfaces and reduce friction and wear. They also act as cooling media and corrosion inhibitors. Common oil and grease lubricants are hydrocarbon products extracted from crude oil. These lubricants work well for their intended purposes, but have inherent limitations. Extreme pressure, temperature, vacuum, radiation and environmental conditions can degrade the lubricating properties of most oil and grease products. Extreme pressure can force oils and greases out of contact areas, while extreme temperatures can reduce the viscosity, causing them to flow away from contacting surfaces. Vacuum can draw and remove lubricants from contacting surfaces, while dusty environments can embed abrasives into lubricants. Space craft operate in extreme environments of temperature, radiation and vacuum.¹⁷ In addition, these unique machines require long-term, single-application lubricants. Service and re-application is not feasible after the craft leaves terrestrial atmosphere. These conditions preclude use of common lubricants and provide an opportunity for bonded solid film lubricants.

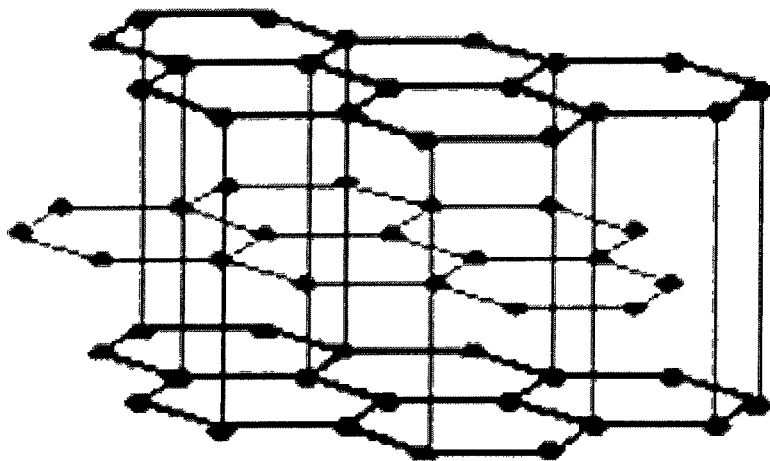
2.4 Dry Film Lubricants

Dry film lubricants are composed of powders with lubricating properties bonded to a surface to provide a low coefficient of friction and good wear preventive action.^{5, 39}

In spite of proven wear resistance, low friction and uses in a myriad of Department of Defense, aerospace and commercial applications, the science and chemistry of dry film lubricants is noticeably sparse in the literature. Much of the best documentation of solid film tribology was conducted before 1970 with little additional advancement since that time.⁴⁴ Lubrication and failure mechanisms of these films are still poorly understood on both microscopic and macroscopic scales.

Unlike their traditional counterparts, dry film lubricants reduce friction and wear between surfaces in rolling and sliding contact without hydrodynamic effects. They lubricate through their lamellar structure, which orient parallel to the surface in the direction of motion, slide over each other, and prevent contact.²⁹ Numerous solid inorganic and organic compounds, as well as certain metals and composite materials have been identified as solid lubricants.¹⁸ Common inorganic solid lubricants are MoS₂, PbO, and hexagonal BN, among others. Organic solid lubricants include polytetrafluoroethylene, phthalocyanine and graphite. Metals such as Ag, Au, Pb and Ba, and composites such as WB-Ag-Ni and Ag-Teflon®-WSe₂ also exhibit lubricating properties.¹¹ Graphite and molybdenum disulfide are the predominant materials used as solid lubricants. Graphite is structurally composed of hexagonal polycyclic carbon planes as illustrated in Figure 2.1. The planes slide one over each other when a lateral shearing load is applied.

Figure 2.1 Lamellar structure of graphite.



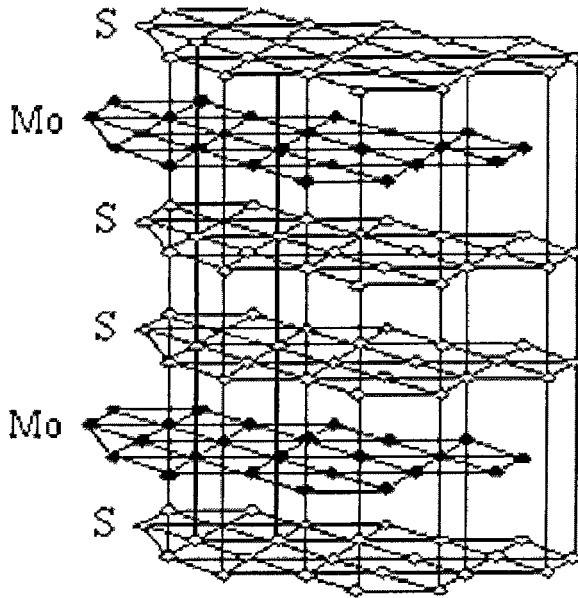
Unfortunately, graphite has been found to induce galvanic corrosion and has been restricted from use in MIL-L-23398.^{6, 7, 12}

2.5 Molybdenum Disulfide

The performance and favorable economics of MoS_2 make it a widely used solid lubricant. Its lamellar, polycyclic crystal structure is similar to graphite, and can slide under an applied load. A structural diagram is illustrated in Figure 2.2.

Calhoun found that it outperformed tungsten disulfide, boron nitride and mica in resin bonded lubricants.¹² Devine examined fifteen metallic sulfides and found that only MoS_2 functioned as a lubricant.¹⁸ MoS_2 is a mineral found in thin veins within granite.³⁸ It is highly refined to achieve purity suitable for use as a lubricant.^{9, 42, 43} The hexagonal crystal structure of MoS_2 has the intrinsic property of easy shear separation between layers.

Figure 2.2 Lamellar structure of molybdenum disulfide.



Walker has postulated that in addition to shearing between layers of sulfur atoms, a certain amount of free sulfur absorbed between the crystal layers act as a lubricant.³⁹ MoS₂ lubrication performance often exceeds that of graphite and is effective in vacuum whereas graphite is not. MoS₂ oxidizes at 400°C, restricting its use to temperatures below that limit. Its load carrying capacity ranges from 225,000 to 500,000 psi, which is beyond the yield strength of many metals. Commercial solid film lubricants often employ a dispersion of MoS₂ and a binding resin.

2.6 Binder Resin Systems

Binder resins utilized in dry film lubricants include inorganic silicates, and organic polymers such as epoxy, urethane, phenolic and polyamide. As in many paint applications, the binder resin dictates the physical, chemical, and performance properties of the final product.^{21, 30, 33} Campbell found solvated polyimide resins in lubricant

applications displayed acceptable performance up to 400°F, but required high cure temperatures. ¹³ Urea resin and MoS₂ provided excellent performance but had poor storage stability, while an epoxy resin lubricant was found to outperform those utilizing silicone, phenolic, furane and urea resins. ¹² Principles of resin polymer chemistry, film formation and adhesion have been extensively studied. ^{25, 31, 32} These resources detail the chemistry and mechanisms that govern many aspects of protective coatings.

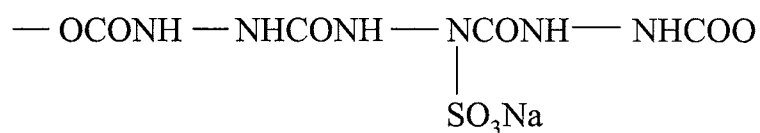
2.7 Waterborne Polyurethane Resin Dispersions

Waterborne polyurethane dispersions have become viable commercial industrial products due to their low VOC content and the quality and performance they offer. Studies have described numerous synthetic processes utilized to prepare ionic, cationic and non-ionic PUD products. ^{10, 16, 20, 22} Recent work has been conducted in non-isocyanate synthesis of urethane dispersions, produced through reaction of cyclic carbonates with diamines. ³⁶ Most urethane dispersions are high molecular weight, ionic polymers where the polyurethane is polymerized in solvent then dispersed in water. Typical urethane dispersions are actually polyurethane-polyurea polymers that contain both the urethane linkage (-NC-CO-NH-) and the urea linkage (-NH-CO-NH-). (Frisch) These moieties are formed by polyaddition between polyisocyanates and polyols leading to polyurethane species, and then reaction of polyisocyanates and polyamines leading to polyurea functionality. A third reaction of isocyanate and water is also involved in urethane dispersion synthesis because the dispersion is offered commercially in aqueous medium. Water reacts with isocyanate groups and produces amines and carbon dioxide *via* the unstable formation of carbamic acid.



The amine groups formed in this reaction can react with remaining isocyanate groups and produce urea linkages. A high degree of urea concentration is desirable because these groups contribute significantly to performance properties. Urea linkages contain two NH functional groups, while urethane contains only one. In this regard, the urea group has twice the hydrogen bonding capability compared to urethane, which leads to improved thermal stability and abrasion resistance of the polymer.

Aqueous polyurethane dispersions are prepared by emulsification of hydrophobic polyurethanes in water with the aid of protective colloids or suitable surfactants. However, the synthetic route yielding a urethane dispersion with an internal hydrophilic group produces a dispersion that does not require strong shear forces during manufacture. In addition, finer particle size, better dispersion stability and reduced water sensitivity of the cured polymer are achieved. Internal ionic dispersants, such as sodium sulfonate (SO_3Na) at 1% by weight, is sufficient to produce stable polyurethane dispersions.



At the interface between the ionic moiety and water, an aqueous-ion double layer is formed by dissociation of the salt group. The counter ion migrates into the aqueous phase. A layer of decreasing electrical charge is formed. Mutual repulsion between like-charge surface layers of different particles is responsible for the stability of the urethane dispersion. The organic binder resin, a key component in development of the DFL product, was a waterborne polyurethane dispersion. Several physical properties and performance characteristics were required of the binder resin for this application. The

resin was to be low in volatile organic content (200 grams-per-liter maximum), free of toxic compounds, able to cure at room temperature in 24-hours or less, and low in viscosity to allow spray application using high-volume, low-pressure (HVLP) spray equipment. The resin had to sufficiently bond to the solid lubricant particle and substrate to which the product was applied. It was required that the cured resin be hard and durable, and resistant to abrasion, moisture, solvents and corrosion. These requirements made waterborne polyurethane dispersion technology an ideal candidate for initial investigations. As improvements to the experimental DFL coating were made, alternative waterborne resin chemistries such as acrylic latex were also evaluated. However, the alternative resins produced inferior endurance life.

2.8 Coalescence

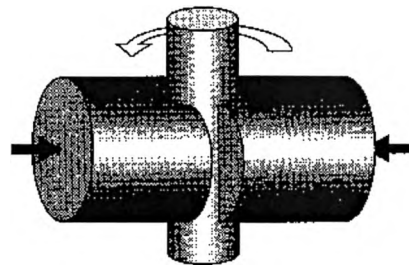
Polyurethane dispersions are well suited for coatings, adhesives and sealant applications.^{15, 23, 37} To form an acceptable film these particles must coalesce and fuse together upon loss of solvent. As water evaporates from the dispersion, the polymer particles must join into a continuous organic phase and co-entangle to provide optimum polymer performance. Coalescing agents are blended into the dispersion and essentially act as volatile external plasticizers.²⁵ They are miscible or partially miscible with the continuous water phase, and remain within the voids between the polymer particles as the water evaporates. They tend to migrate into the polymer particles, causing them to swell, which assists with the fusion of the discrete particles into a cohesive film. Coalescing aids such as N-methylpyrrolidone (NMP), tripropyleneglycol (mono) methyl ether (TPM) and dipropyleneglycol normal butyl ether (DPnB) have higher boiling points than water

and are often added to urethane dispersion products to enhance coalescence and film formation.

2.9 Falex Pin and Vee Block Tester

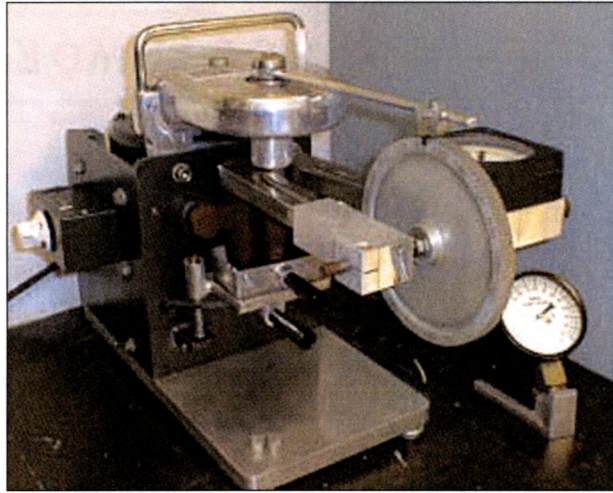
Most performance evaluations of the DFL coating utilized the laboratory-scale Falex Pin and V-Block tester. This device has been a staple in the lubricants industry for decades and is used to determine endurance life and load carrying capacity of oils, greases and solid lubricants.⁴⁰ Tests are typically performed following ASTM D2625 procedures.³ The Falex machine applies a lateral load to two blocks with grooves in their faces, between which a pin is inserted and rotated.³⁹ Figure 2.3 is an illustration of contacting pin and vee blocks.

Figure 2.3 Falex pin and vee block design.



The pin is rotated and the torque is measured. When the torque increases, this indicates the coating has worn through and the test is terminated. The wear life of the lubricant is the time recorded to test termination. Figure 2.4 is a photograph of the Falex pin and vee block tester.

Figure 2.4 The Falex pin and vee block tester.



To prepare for the test, the steel pin and vee block sets are grit-blasted, then coated with the lubricant. After 24-hour room-temperature cure the set is installed into the machine. The machine is started and rotates the pin at 290 revolutions per minute. The load is gradually applied during the first five minutes of the test, which is referred to as the break-in period. After this the load is increased to 1000-pounds and the machine is allowed to run until the coating fails. Three indicators constitute a failure. These are: (1) a torque increase of ten inch-pounds above the “steady-state” value, (2) seizure or breakage of the coated pin, or (3) breakage of the brass locking pin that retains the pin in the chuck of the machine. Military specification MIL-L-23398 requires that the lubricant endure for 60 minutes at the 1000-pound applied load.

According to MIL-L-23398, a load carrying capacity test is also required of the lubricant using the Falex machine. The procedure is also described in ASTM D 2625.³ In this test a coated pin and vee block set is to sustain an applied load of at least 2500-pounds for one minute prior to failure.

In this test a coated pin and vee block set is to sustain an applied load of at least 2500-pounds for one minute prior to failure.

2.10 Corrosion Control

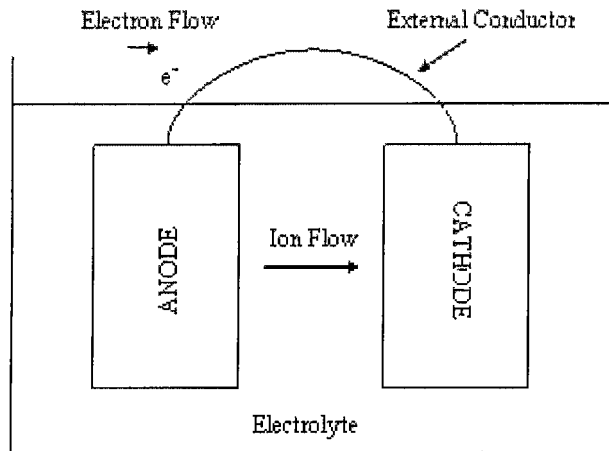
An equally important requirement of the lubricant is substrate protection from corrosion. A comprehensive study conducted by the Society for Protective Coatings (SSPC) reported that annual metallic corrosion costs in the United States eclipse \$300 billion.³⁵ In an effort to address potential corrosion of lubricated metal parts, military specification MIL-L-23398 includes a corrosion protection requirement.

Corrosion of metals is a complex process defined as “the chemical or electrochemical reaction between a metal and its environment resulting in the loss of the material and its properties.”⁴ Corrosion is a natural process of returning refined, high energy metals (both pure and alloy) to their original lower energy state.²⁴ A classic example is the life cycle of iron and steel. Mined iron ore is very stable, low energy iron oxide (FeO, Fe₂O₃, Fe₃O₄). Construction grade iron is made in a high energy “smelting” process that drives off oxygen, resulting in elemental iron. This form is not stable. Presence of water and oxygen can readily reverse the process resulting in formation of iron oxide.

Corrosion occurs through the action of an electrochemical cell.¹⁹

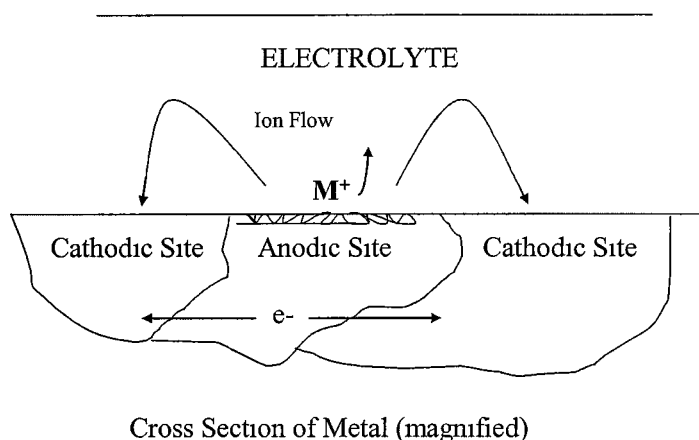
A simple cell, illustrated in Figure 2.5, is composed of an anode, a cathode, an electrolyte and a conductive path for the flow of electrons. Corrosion occurs at the anode when all four components are present.

Figure 2.5 Components of an electrochemical cell.



Rigorous treatments of this topic can be found in publications by the Society for Protective Coatings (SSPC) and the National Association of Corrosion Engineers (NACE). An electrochemical cell can form on the surface of a metal in various environments and induce corrosion. The location of the anode and cathode on the surface shifts during exposure as the process continues. The external conductor (metallic path) is through the metal itself. Ions dissolved in atmospheric moisture function as the electrolyte. Figure 2.6 is a schematic section of metal. The surface has become an electrochemical cell and is being corroded at the anode site.

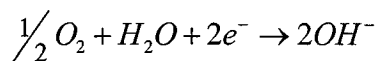
Figure 2.6 Corrosion can occur on the surface of a metal that has become part of an electrochemical cell.



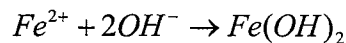
Three distinct steps occur during corrosion of iron. First, elemental iron is oxidized to the +2 state, which is soluble in water.



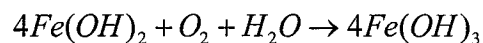
Simultaneously, two electrons are released and migrate through the metal to the cathodic site. The electrical circuit is complete when oxygen in the water migrates to the cathode and uses the electrons to form hydroxyl ions (OH^-).



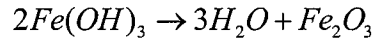
The negatively charged hydroxyl ions move toward the anode, and positively charged iron ions toward the cathode. They combine to produce ferrous hydroxide.



The ferrous hydroxide is further oxidized to ferric hydroxide.



Ferric oxide (red rust), the original low energy iron state is the final product when the ferric hydroxide is dehydrolyzed.



Elimination of ionic species, oxygen and water through the use of protective paints reduce these reactant concentrations at the metal surface.²⁵ Many coatings are not completely impervious to water, but are very effective at reducing the concentrations of ionic species generated by the cell. Mayne has shown that the rate of ionic diffusion through barrier films was much lower than diffusion of water.²⁹ Corrosion is therefore diminished through reduced activity of reactants and the respective reaction products.

2.11 Design of Experiments

A design of experiments (DOE) was constructed as lubricant performance improved. A DOE is a small set of devised experiments in which all pertinent factors are varied systematically.^{26,27} Analysis of the resulting experimental data can identify optimal conditions, the factors that most influence the results and those that do not, and the presence of interactions between factors. The data are analyzed and provide a model relating the factors to the results, showing which factors are important, and how they combine to influence the results. The model is then used to make predictions of factor setting to achieve optimum results.

The most important aspect of design of experiments is that it provides a strict mathematical framework for changing all pertinent factors simultaneously, and this is accomplished in a small number of experimental trials.

2.12 Characterization

Upon successfully meeting all requirements of MIL-L-23398, the product was characterized by optical microscopy, Fourier transform infrared spectroscopy (FTIR), x-ray photoelectron spectroscopy (XPS) and atomic force microscopy (AFM). Optical microscopy examined visual details of the pin and vee block sets at various stages of wear. The XPS, AFM and FTIR experiments were performed on pin specimens after various stages of endurance life wear. A pristine, unworn pin served as a control. A second pin was subjected to mild wear conditions during the break-in period. A third pin was worn under extreme pressure conditions for 30-minutes, while the fourth pin was worn until lubricant failure. Identification markers were scribed onto each specimen to ensure that XPS, AFM and FTIR techniques examined the same area on the individual pins

CHAPTER 3

EXPERIMENTAL

3.1 MIL-L-23398 Solid Film Lubricant Performance Specification

The basis of the test methodology to development the dry film lubricant was dictated by Military Specification MIL-L-23398D. It established the requirements for the air-cured solid film lubricant as a bulk dispersion (Type I) and aerosol propelled (Type II) product form. Section 3.4 of the specification outlines the required performance characteristics and serves as a principle guide for product development. The requirements are summarized in Table 3.1

Table 3.1 MIL-L-23398D performance requirements.

MIL-L-23398D Requirement	Performance Characteristic	Description
3.4.1	Film Adhesion	ASTM D2510 – Standard Test Method for Adhesion of Solid Film Lubricants
3.4.2	Resistance To Fluids	Lubricant is to maintain adhesion per ASTM D2510 after immersion in nine different fluids including hydrocarbon oils, fuel, cleaning compounds, anti-icing fluid, silicone fluid and reagent water.
3.4.3	Thermal Shock Sensitivity	ASTM D2511 - Determine resistance of the lubricant to deterioration when subjected to temperature extremes.
3.4.4	Endurance Life	ASTM D2625, Procedure A – Determine lubricant performance life in the Falex Pin and V-Block extreme pressure test.
3.4.5	Load Carrying Capacity	ASTM D2625, Procedure B – Determination of the maximum load that the DFL can sustain in the Falex Pin and V-Block extreme pressure test.
3.4.6	Aluminum Corrosion Resistance	ASTM D2649 – Aluminum test panels coated with the DFL are exposed in a salt fog corrosion chamber for 500 hours (21 days).
3.4.7	Sulfurous Acid – Salt Spray	Federal Standard 791-533 – Steel specimens coated with the DFL are exposed to sulfurous acid – salt spray, and shall resist pitting, corrosion and staining.
3.4.8	Spray Duration and Pattern (Type II only)	Aerosol propelled DFL shall have a 1.5-inch width and be effective for 270 seconds.
3.4.9	Storage Stability	A liquid sample of the bulk DFL product is to be stored at 25°C for a period of one year. Endurance life and sulfurous acid – salt spray properties are to be met with the aged product.

Solid lubricant pigments, binder resins, solvent (water) and film forming additives (surfactants, coalescent agents, corrosion inhibitors, pH adjusters, *etc.*) were formulated

into an optimized blend to meet requirements. Lab batches of 100-gram quantities were easily produced using high-shear blending of the mixtures. Modifications were initially performed in an iterative manner of hypothesis, experimentation, and analysis of results, followed by new hypothesis. This research and development was conducted over a 24-month period, during which approximately 420 formulations were prepared and evaluated.

Initial efforts focused on meeting the 60-minute endurance life requirement with a waterborne dry film lubricant coating. After six months of development, a formulation was identified that could meet and exceed this. Unfortunately, this formulation provided poor corrosion protection. The remaining 18-months focused on modifying the initial formulation to develop the required corrosion resistance, while maintaining endurance life. Midway through the latter undertaking it became apparent that corrosion resistance improvements directly diminished endurance life. However, optimization of the coating solids content, removal of corrosion inducing additives and balancing coalescing agents substantially improved corrosion resistance and endurance life.

3.2 Silicate Based Lubricants

Experimental lubricant coatings based upon silicate binders with molybdenum disulfide, boron nitride and polytetrafluoroethylene (PTFE) lubricants were prepared and initially evaluated for endurance life. Descriptions of the formulations are presented in Table 3.2. Aqueous sodium silicate is a solution of glasses composed of SiO_2 and Na_2CO_3 , known as “water glass”. These convert to solid films upon evaporation of water. Inferior wear and endurance life were observed with this binder. Coatings wore through

early in the test, even during the break-in period at low pressure (300 lb. Load), and were not able to carry a load.

Table 3.2 Silicate-based solid film lubricants.

Formulation ID	Composition
A2162-3-25 A2162-7-8 A2162-9-5 A2162-9-17 A2162-9-28 A2162-11-11 #1 A2162-11-11 #2 A2162-13-8B	Combinations of liquid sodium silicate binder, hexagonal boron nitride lubricant, surfactant and water.
A2162-19-20 #1	MoS ₂ replaces BN as the solid lubricant
A2162-19-20 #2	MoS ₂ and PTFE solid lubricants
A2162-25-13	PTFE solid lubricant
A2162-25-21	PTFE and BN solid lubricants

Close examination of the silicate coatings revealed brittle films with no cohesive strength after room-temperature cure. This and the persistent problem of premature coating wear lead to a search for alternative binder resins.

3.3 Polyurethane Dispersions

Polyurethane binder resins have proven performance histories in coating applications that require superior resistance to abrasion and corrosion. Several manufactures provided samples of commercial urethane resins that were all similar in solids content, pH and N-methylpyrrolidone (NMP) co-solvent content. These products are listed as the first ten materials in Table 3.3.

Table 3.3 Materials obtained for evaluation

Component	Function	Supplier
Joncryl U-4188	Urethane Resin	Johnson Polymer
Joncryl U-4100	Urethane Resin	Johnson Polymer
Joncryl 2561	Urethane Resin	Johnson Polymer
Hybridur 541	Urethane Resin	Air Products
Hybridur 570	Urethane Resin	Air Products
Macekote 5218	Urethane Resin	Mace Adhesives
Macekote 8538	Urethane Resin	Mace Adhesives
Macekote 8539	Urethane Resin	Mace Adhesives
Hauthane HD-2107	Urethane Resin	C.L. Hawthaway
Hauthane HD-2503	Urethane Resin	C.L. Hawthaway
Spensol F-97	Oil-modified Urethane	Reichold
De-ionized Water	Diluent	TRI/Austin
Arcosolv DPNB	Co-solvent	Arco Chemical
Arcosolv TPM	Co-solvent	Arco Chemical
Disperbyk	Dispersion Agent	BYK Chemie
BYK-346	Dispersion Agent	BYK Chemie
BYK-348	Dispersion Agent	BYK Chemie
Foam Ban 247	De-Foaming Agent	Ultra Additives Inc.

Molybdenum Disulfide	Lubricant	Atlantic Equipment Engineers
Hexagonal Boron Nitride PT140	Lubricant	Advanced Ceramics Corp.
Mica	Lubricant	Zemex Industrial Minerals
Teflon Powder (1 μ m)	Lubricant	Aldrich Chemical Co.
Monoethanol amine	Corrosion Inhibitor	Aldrich Chemical Co.
Triethanol amine	Corrosion Inhibitor	Aldrich Chemical Co.
Morpholine	Corrosion Inhibitor	Aldrich Chemical Co.
Ammonia	Neutralizer	Aldrich Chemical Co.
Zinc Oxide / Zinc Molybdate	Corrosion Inhibitor	Sherwin Williams
Zinc Phosphate	Corrosion Inhibitor	Rockwell Minerals
Zinc Salt of an Organic Nitro Compound	Corrosion Inhibitor	Heubach Corporation
Calcium Phosphosilicate	Corrosion Inhibitor	Halox Corporation
Strontium Zinc Phosphosilicate	Corrosion Inhibitor	Halox Corporation

As with many paint and coating formulations, additives were incorporated into the experimental DFL product. These included surfactants to enhance flow, leveling and wetting of the coating. Also included were de-foaming additives and butyl ether coalescing solvents to aid in film formation. The additives evaluated are presented in Table 3.3.

To list all of the formulations evaluated in this effort would be exhaustive. However, details of key formulations will be presented to provide an in-depth chronology of the development process.

Formulations based upon Joncryl U-4188 as the binder resin consistently produced coatings that were able to reach and maintain the required 1000-pound applied load before failing the endurance life test. Table 3.4 lists the formulation, pigment-to-binder ratio, solids content and endurance life of key experimental lubricants that

outperformed the silicate-based lubricants in Table 3.2. Formulation A2171-107A withstood the 1000-pound load for approximately three minutes before failure. While endurance life was well short of the requirement, it was an improvement over the silicate based systems and an early indication that the polyurethane dispersion was feasible as the binder resin.

Table 3.4 Lubricants based upon urethane resin with improved endurance life.

Formulation ID	Composition	Pigment to Binder Ratio	Percent Solids	Endurance Life (minutes)
A2171-75C	Urethane Resin DPnB TPM Polysiloxane defoamer Silicone surfactant DI Water MoS2 Boron Nitride	5 : 1	29	1
A2175-107	Same as A2171-75C with Mica replacing Boron Nitride	5 : 1	23	3

Commercial solid film lubricants were also evaluated to obtain benchmarks for endurance life, with results listed in Table 3.5. Comparison of formulation A2171-107A to a solvent-based commercial product, EM-PS-G, revealed that the experimental waterborne system outperformed the solvent-based system. Several commercial water-based products outperformed A2171-107A in endurance life, but were also well short of the 60-minute requirement.

Table 3.5 Endurance life performance of commercial lubricants.

Competitive DFL Product	Composition	Endurance Life (minutes)
Commercial Product T	Waterborne	5
Commercial Product PL 99	Waterborne	3
Commercial Product EMPS-G	Solvent Based	0
Commercial Product LL-2396	Waterborne	10

Further investigations revealed poor corrosion resistance of the commercial waterborne products. Tests for endurance life were curtailed when development shifted to address poor corrosion resistance of the lubricant. A lengthy period was spent pursuing acceptable corrosion resistance. Those efforts are detailed in Chapter 3.4. Seven notable lubricant formulations are listed in Table 3.6. Outstanding endurance life but poor corrosion resistance was observed with formulations A2192-37 and A2192-55. The reverse trend was seen with A2200-13. A design of experiments, described in Chapter 4, revealed resin, lubricant and additive levels were near optimum with A2200-13. Series A2200-61 revealed that powdered polytetrafluoroethylene (PTFE) greatly reduced the measured torque during break in for endurance life. This suggested that PTFE could minimize early formation of lubricant point defects under extreme pressure. Final pigment-to-binder ratio and solids content optimizations were made, culminating with formulation A2200-69A. Highlighted in Table 3.6, the lubricant was capable of simultaneously meeting the two most difficult requirements of MIL-L-23398. The new lubricant was fully evaluated and found to meet or exceed the remaining requirements. An independent laboratory confirmed the product performance. Spectroscopic techniques were employed to characterize subtle mechanisms of lubrication, friction and

wear inherent to the product, and presented in Chapter Five. Due to the novelty of this lubricant, a U.S. Patent application was filed.⁸

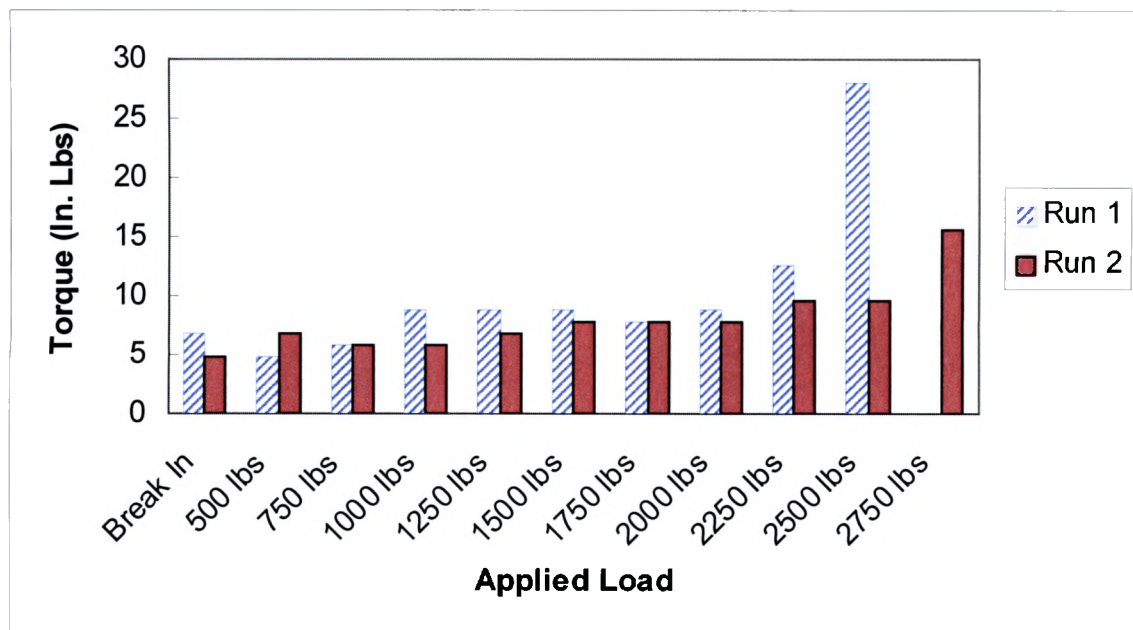
Table 3.6 Compositions, parameters and performance of seven key formulations.

Formulation ID	Basic Formulation	Pigment to Binder Ratio	Percent Solids	Endurance Life (minutes)	Corrosion Resistance
A2192-37	DI Water Polysiloxane Defoamer Ammonia Molysulfide Oil Modified Urethane Co-Urethane Resin Biodegradable Surfactant Drying Agent	4 to 1	20	90	Poor
A2192-55	DI Water Polysiloxane Defoamer Ammonia Molysulfide Urethane Resin TPM DPnB Surfactant	5 to 1.5	21	111	Poor
A2200-13	DI Water Polysiloxane Defoamer Molysulfide Ammonia Urethane Resin Surfactant TPM DPnB	5 to 3 1	34	25	Outstanding
A2200-61A	A2200-13 Plus Boron Nitride	5 to 2.5	39	14	Outstanding
A2200-61B	A2200-13 Plus Mica	5 to 2 5	39	16	Outstanding
A2200-61C	A2200-13 Plus PTFE	5 to 2.5	39	33	Outstanding
A2200-69A FINAL OPTIMIZED FORMULATION	DI Water Ammonia Urethane Resin Molysulfide PTFE Surfactant TPM DPnB	5 to 3.2	34	63	Outstanding

3.4 Load Carrying Capacity

A test to measure maximum load the lubricant could support without failure or excessive wear was conducted. The determination was made following ASTM D 2625. The test was similar to endurance life, but differed by increasing applied load 250 pounds per minute until lubricant failure. The lubricant is required by MIL-L-23398 to reach and sustain 2500 pounds. Evaluations of lubricant A2200-91 revealed its capability of meeting the requirement. Figure 3.1 is a plot of the Falex machine torque as a function of applied load, indicating lubricant performance.

Figure 3.1 Lubricant A2200-91 met 2500-pound load carrying capacity requirements of the specification.



Specimen 1 met the requirement but could not sustain a load beyond 2500 pounds.

Specimen 2 sustained 2750-pounds for one minute before lubricant failure.

3.5 Endurance Life and Temperature Effects

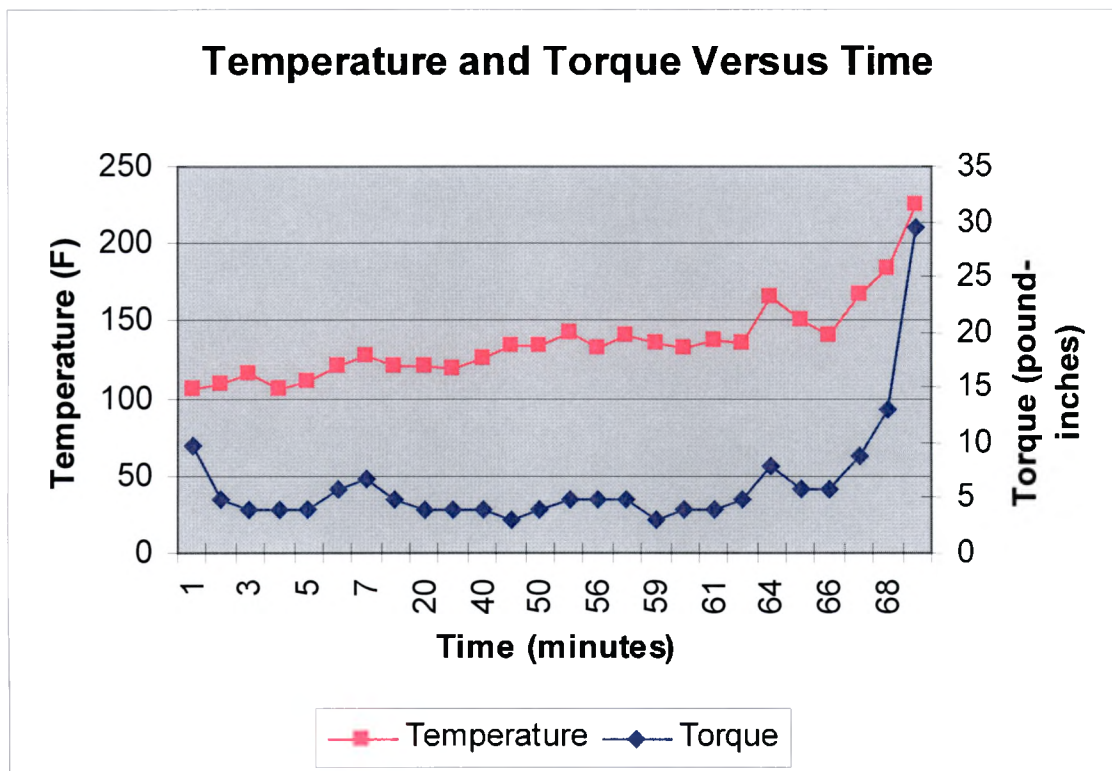
Experience in conducting the endurance life test taught that the pin and vee block assembly accumulated substantial heat during the course of the test. It was thought the specimen temperature might get hot enough to initiate decomposition of the coating, lubricant or both. So, a study was conducted to determine the temperature profile of formulation A2200-91, during repeat of the test. A hand held, non-contact infrared thermometer with laser pointer was used to measure temperature on the surface of the rotating pin. Figure 3.2 depicts the pyrometer and a detailed view of the laser point on the exposed surface of the rotating pin.

Figure 3.2 A digital pyrometer with laser pointer.



Torque on the Falex machine motor was simultaneously recorded to monitor lubricant performance. The pin surface temperature and machine torque were plotted as functions of time during the test. A plot in Figure 3.3 shows that under extreme pressure, temperature remains relatively constant between 105 and 140 °F during the required 60-minute duration. The temperature remained at least 200 °F below the decomposition point of the urethane resin.

Figure 3.3 Temperature and torque measurements during the endurance life test.



After 64-minutes, a rise in torque and temperature is evident. The rapid increase indicated onset of coating failure. Temporary decreases in temperature and torque at 65 and 66 minutes may have been residual MoS₂ briefly filling the initial point of failure. However, rapid and simultaneous increase of torque and temperature at 68 and 69 minutes indicated the coating completely wore through and could no longer sustain the load.

3.6 Corrosion Control

The primary function of the DFL focused on tribological aspects that include lubrication, a low coefficient of friction (COF), endurance life and load carrying capacity. An equally important requirement of the coating is corrosion protection of the substrate.

3.6.1 Salt Fog Corrosion Resistance

Laboratory testing involved salt fog exposure of coated steel panels for assessment of corrosion resistance. A detailed analysis of the base formulation was conducted to identify components that were detrimental to the corrosion protection of the coating. The analysis consisted of coating steel test panels with the experimental products, placing them into a salt fog chamber, and evaluating them every 24 hours up to the specified 100-hour total exposure. Figure 3.4 is a photo of the salt fog cabinet that was operated according to ASTM B117 procedures and used for the analysis.

Figure 3.4 Salt fog chamber during sample inspection.

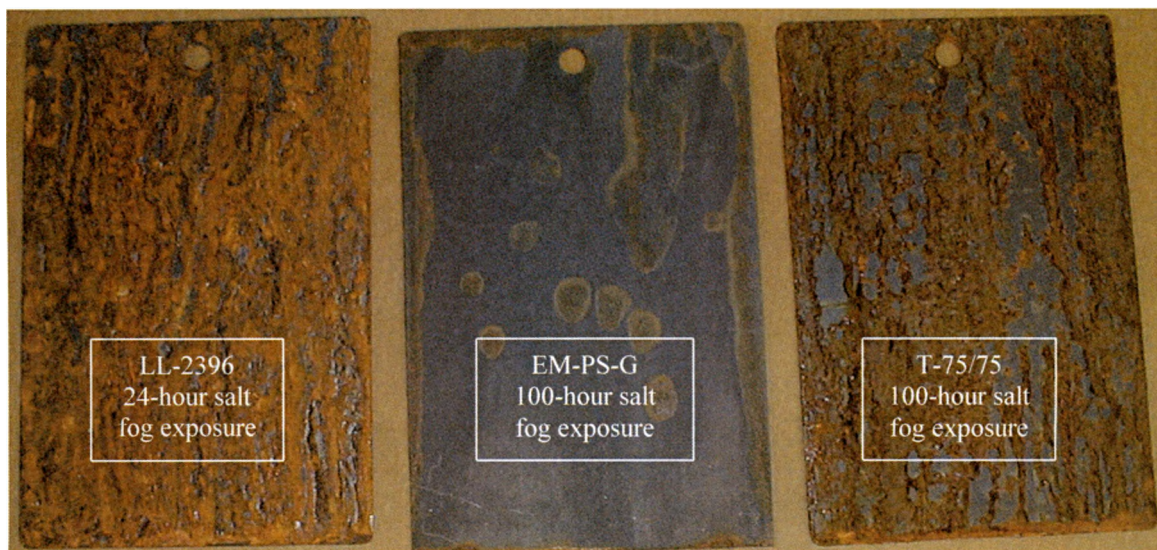


3.6.2 Commercial Product Corrosion Analysis

Cold rolled steel test panels from ACT Laboratories (#APR 10159) were used to screen candidate formulations. Phosphate treated test panels (ACT #APR 1903), as prescribed by the specification, were used to evaluate promising formulations that showed potential in the screening phase. Three commercial dry film lubricants were initially evaluated to establish a benchmark. Waterborne products LL-2396 and T-75/75, and solvent based EM-PS-G were applied to panels and cured at room temperature for seven days. The panels were placed into the cabinet and monitored. Figure 3.5 is a

photograph that illustrates the degree of corrosion that occurred. LL-2396 severely corroded after 24-hours of exposure, while T-75/75 exhibited corrosion on approximately 80% of the panel after 100 hours. EM-PS-G had eight distinct corrosion spots on the panel surface after exposure. The requirement to pass MIL-L-23398 allows no more than three corrosion spots with a maximum diameter of one-millimeter after exposure.

Figure 3.5 Corrosion test panels coated with commercially available dry film lubricants after salt fog exposure.



Corrosion resistance evaluations were also conducted on the formulation that met endurance life requirements. Results indicated poor corrosion protection of the substrate. Figure 3.6 is a photograph that depicts the degree of corrosion after exposure.

Figure 3.6 Corroded test panel after salt fog exposure.



3.6.3 Corrosion Inhibitor Analysis

Corrosion inhibitors commonly found in waterborne paints to enhance the corrosion resistance of cured films that contain them were evaluated. Amine andazole inhibitors showed no improvements, as evidenced by the picture in Figure 3.7. Additional corrosion inhibitors based upon zinc, amine and phosphate chemistries were evaluated, but did not provide improvements. Most of the additives were incompatible with the system and caused rapid agglomeration or increased product viscosity.

Figure 3.7 Corroded panel with lubricant containing corrosion inhibitors.



The inability of the lubricant to provide corrosion protection suggested formula changes were required. Efforts were made to retain the urethane resin and molysulfide combination due to the endurance life provided. Commercially available corrosion control additives, listed in Table 3.7, were incorporated into the formulation but did not improve the performance.

Table 3.7 Summary of corrosion control additives.

Formulation	Description	Results
A2176-109	Similar to initial formulation but uses morpholine as neutralizer and corrosion inhibitor.	Rapid corrosion occurred in salt fog test.
A2176-123 A	Triethanol amine used as a neutralizer and corrosion inhibitor.	No improvements in the corrosion protection.
A2176-123 G	Diethanol amine used as a neutralizer and corrosion inhibitor.	No improvements in the corrosion protection.
A2176-129 A	Azole corrosion inhibitor with triethanol amine as the neutralizer	Severe corrosion observed after 24 hour exposure time.
A2176-129 B	Azole corrosion inhibitor monoethanol amine as the neutralizer	Severe corrosion observed after 24 hour exposure time.
A2176-129 C	Azole corrosion inhibitor with diethanol amine as the neutralizer	Severe corrosion observed after 24 hour exposure time.
A2176-137 A	Analysis of zinc phosphate, zinc salt and zinc oxide corrosion inhibiting additives into base formulation, Joncryl used as binder resin.	Formulation not stable. Rapid disruption of the dispersion, rapid thickening.

A2176-137 B	Analysis of zinc phosphate, zinc salt and zinc oxide corrosion inhibiting additives into base formulation, Hybridur used as binder resin.	Formulation not stable. Rapid disruption of the dispersion, rapid thickening.
A2176-141 A	Zinc phosphate, zinc salt in Joncryn base formulation.	Severe surface corrosion after 24 hour exposure.
A2176-141 B	Zinc phosphate, zinc salt and Hybridur base formulation.	Severe surface corrosion after 24 hour exposure.
A2176-147 A, B, C	Introduction of strontium zinc phosphosilicate corrosion resistance additive into Joncryn based formulation	Formulation not stable. Rapid disruption of the dispersion, rapid thickening.
A2176-147 A, B, C	Introduction of calcium phosphosilicate corrosion resistance additive into Joncryn U-4188 based formulation	Formulation not stable. Rapid disruption of the dispersion, rapid thickening.
A2178-33 A thru H	Re-evaluation of HALOX corrosion additives, and four best urethane binder resins.	Reduction of corrosion to light and moderate levels. Test panel 33 G found to be free of blisters and free of corrosion.

Testing revealed silicone surfactants and defoaming additives induced corrosion through an unknown mechanism. Table 3.8 lists formulation number, additive employed and observed exposure results.

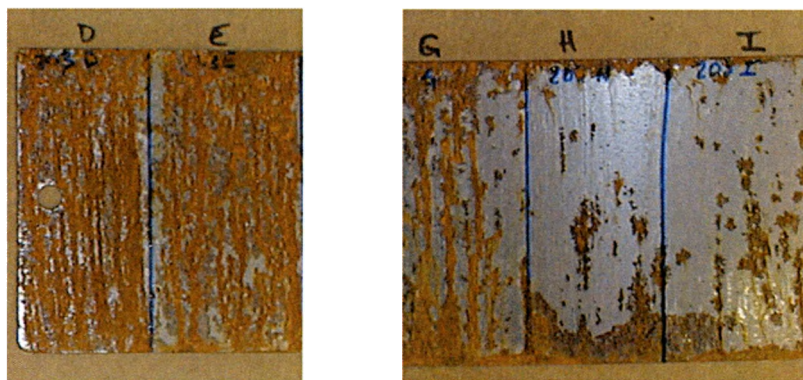
Table 3.8 Summary of surfactant additives.

Formulation	Description	Results
A2176-187	Individual components, separately evaluated in the Hybridur resin	Resin (alone) – No corrosion Resin/Water – Moderate Corrosion Resin + Additive #1 – Moderate Corrosion Resin + Additive #2 – Severe Corrosion Resin/Molysulfide – Staining/Light corrosion Resin/ammonia – Light corrosion Resin/Surfactant – Severe corrosion

		Resin + Coalescent #1 – Light corrosion Resin + Coalescent #2– Light corrosion
A2176-203	Analysis of alternative defoamers (9)	Three products found to be acceptable. All others were poor.
A2178-09	Analysis of defoamers	One found to be more efficient.
A2178-17	Analysis of emulsion additives.	Rapid formation of blisters in salt fog cabinet. Rapid corrosion occurred.
A2178-31	Analysis of defoamer and Envirogem AE-01 surfactant.	Addition of defoamer caused rapid, heavy corrosion to form. Addition of surfactant showed reduced blister and corrosion formation.

Surfactant additives are necessary in waterborne coatings to obtain acceptable performance. However, silicone-containing additives in the lubricant had a detrimental effect on the corrosion protection of steel. Literature searches and product evaluations identified alternatives that did not diminish the protection capacity of the coating. Envirogem AE-01, an external surfactant based upon proprietary, biodegradable chemistry offered flow, leveling and de-foaming improvements to the lubricant coating without causing corrosion. Figure 3.8 shows reduced corrosion in regions H and I on the panel surface, versus regions A, D and E which used silicone based surfactants.

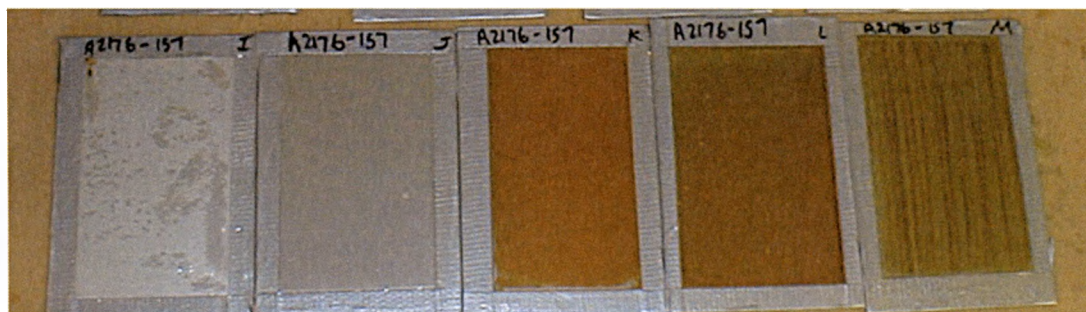
Figure 3.8 Coated panels with various levels of corrosion.



3.6.4 Binder Resin Analysis

Analysis of several binder resins, applied neat, revealed varying degrees of corrosion resistance. Figure 3.9 is a photograph of 13 waterborne resins prior to exposure. Eight urethane coatings in the upper two rows of the photo formed clear films. An acrylic emulsion, bottom row left, embrittled and cracked during cure. Interestingly, two polyurethanes and one acrylic corroded the metal surface during cure, as evidenced by three discolored panels.

Figure 3.9 Waterborne resins applied neat over steel panels.



Four of 13 resins provided acceptable corrosion resistance after exposure. Included are urethane dispersions Joncyl U-4188 and Macecoat 8539, Spensol F-97 oil-modified urethane dispersion, and Hybridur 570, a hybrid urethane/acrylic dispersion.

Descriptions of the resins, formulations and corrosion resistance results are listed in Table 3.9. The positive results suggested that waterborne urethane films are capable of corrosion protection and were good resin candidates for the lubricant.

Table 3.9 Urethane resin analysis and observed results after testing.

Formulation	Description	Results
A2176-157 A thru M	13 different urethane binder resins analyzed.	Four different products show excellent corrosion resistance.
A2178-53 A thru E	Evaluation of modified A2178-33 G formulation using blends of two best binder resins.	Moderate to heavy corrosion observed on steel test panels after exposure.

3.6.5 Solids Content and Corrosion Resistance

A series of experiments were also conducted to determine corrosion resistance as a function of total solids content in the cured film. That test proved valuable as it identified a lower and upper threshold content, outside which corrosion protection rapidly diminished. De-ionized water was used to dilute the solids content of urethane resin. Results are summarized in Table 3.10. The solids content ranged from 6 to 38 percent. The optimum was 24 percent. Specimen A2176-205-A was the neat resin with maximum solids content of 38 percent. Specimen A2176-205-E, with a solid content of 24% revealed near-optimum level. An abrupt increase in corrosion occurred with specimen A2176-205-F and continued throughout the remainder of the series.

Table 3.10 Summary of solids content and corrosion

Sample ID	Percent Solids	Corrosion on Panel Surface (%)
A2176-205-A	38.0	95
A2176-205-B	35.0	85
A2176-205-C	34.0	80
A2176-205-D	30.0	50
A2176-205-E	24.0	40
A2176-205-F	22.0	90
A2176-207-A	20.0	100
A2176-207-B	18.0	95
A2176-207-C	15.0	90
A2176-207-D	13.0	100
A2176-207-E	10.0	100
A2176-207-F	6.0	100

3.6.6 Glycol Ether Coalescents

Detailed studies were conducted on glycol ether coalescent additives. These studies proved valuable as they identified optimum blend levels of tripropyleneglycol mono-butyl ether (TPM) and dipropylenglycol normal-butyl ether (DPnB). Table 3.11 lists the coalescent blend modification and effect on corrosion resistance. The optimum blend simplified the formulation mixing process, improved wetting, eliminated coating defects and increased product stability.

Table 3.11 Effect of coalescent blends *versus* corrosion.

Formulation	Description	Results
A2178-171 A	Removal of Dispersant and one coalescent additive from Joncryl based formulation.	Severe corrosion after 72 hours of exposure
A2178-171 B	Removal of Disperbyk 190 and two coalescent additives from Joncryl based formulation.	Severe corrosion after 72 hours of exposure
A2178-61 A thru F	Evaluation of coalescent additive blend ratios.	Sample 61 F shows excellent resistance after 24 hours of exposure. Others in the series do not do as well.
<i>A2178-67</i>	Further coalescent additive blend ratio studies.	Sample 67B shows excellent performance in blister reduction and corrosion protection.

3.6.7 Formulation Modifications

After detailed analysis of the findings above (resin type, solids content, additive type and levels and coalescent blend), changes were made to incorporate individual improvements into a synergistic blend. Series A2178-75, 95 and 97 incorporated the changes and were tested for corrosion resistance. The performance was outstanding and met specification requirements. Figures 3.4-7 is a photograph that shows the corrosion

protection offered by the modified formulation after exposure. The staining on the panels in Figure 3.11 resulted from exposed, cut edges of the panel.

Figure 3.10 Series A2178-75 provided outstanding corrosion protection after 100 hours of salt fog exposure.



Unfortunately, formulation A2178-75 was not stable and gelled after aging. An incompatibility between one of the formulation binder resins and either the coalescent products or the molysulfide lubricant was suspected. Attempts were made to alleviate the instability through alternative coalescent aids. Removal of TPM and DPnB resulted in poor surface wetting and film formation, slower dry times, and reduced endurance life. In addition, the absence of TPM and DPnB caused the product to foam during mixing. Observations revealed the necessity of these products for surface tension reductions and optimum resin particle coalescence.

It was also postulated that molysulfide was incompatible with one or more components. To determine this possibility, molysulfide was replaced with hexagonal boron nitride in formulation A2178-207A, while A2178-111 did not contain a lubricating

pigment. Both were found to be stable for over four months and continue to show no sign of viscosity increases or instability. Those results suggest incompatibility between one of the co-resins the molysulfide lubricant.

3.6.8 Urethane and Acrylic Co-resins

A waterborne acrylic resin with cited corrosion protection properties was blended with a polyurethane resin. The acrylic was found to be compatible and did not affect product stability. After 100 hours of salt fog exposure the coating did not exhibit the extent of corrosion that occurred on previous test panels. Figure 3.12 is a photograph of a panel after exposure.

Figure 3.11 A urethane/acrylic resin blend.



Unfortunately, the endurance life dropped from 90 minutes to seven with the addition of the acrylic. It was suspected that the acrylic may not bond effectively to molysulfide, causing reduced endurance life.

3.6.9 Final Formula Optimization

Continued analysis of product stability revealed lubricant formulations based upon Joncryn U-4188 resin were stable after six month shelf life aging. Review of series A2176-157 showed that of the 13 resins analyzed it provided optimum corrosion protection. These two attributes made Joncryn U-4188 the resin of choice for the remainder of the investigation. Formulation A2200-13 combined near optimized solids levels and coalescent blend, a non-silicone surfactant and Joncryn U-4188. The corrosion resistance offered by the lubricant was outstanding. However, the endurance life of the product was only half the required performance.

Further enhancements of formulation A2200-13, through the incorporation of powdered polytetrafluoroethylene, were found to simultaneously provide the required corrosion protection and endurance life. The converging requirements were finally met with formulation A2200-69A.

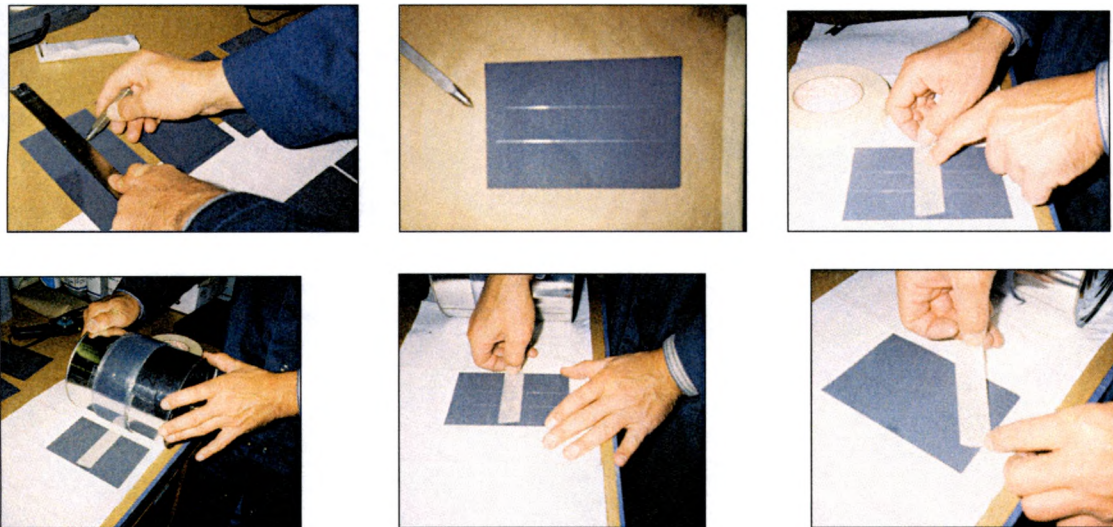
Table 3.12 Tabulated results of final formula optimization that produced the target lubricant.

Formulation	Description	Results
A2200-13	Joncryn U-4188 resin, refined solids content and coalescent blend, elimination of silicone surfactants.	Outstanding Corrosion Resistance. Endurance Life of 37-Minutes
A2200-69A	DI Water Ammonia Joncryn U-4188 Molysulfide PTFE Envirogem AE-01 Surfactant TPM DPnB	Outstanding Corrosion Resistance and Endurance Life of 63-Minutes

3.7 Adhesion and Chemical Resistance

Simultaneous achievement of endurance life and corrosion resistance provided by formulation A2200-69A signaled near completion of the product development. Six requirements of lesser challenge remained. Included were film adhesion, chemical resistance to nine different fluids, thermal shock sensitivity, aluminum corrosion resistance, sulfurous acid salt spray resistance, and storage stability. Fluid resistance was performed in conjunction with the adhesion test following ASTM D 2510 procedures.¹ In the adhesion test the lubricant is applied to a steel panel and cured for six hours. A pointed metal awl is used to scribe two horizontal lines through the coating. Tape is placed over the scribed lines, pressed with a two pound roller, and quickly removed from the coating surface. The test procedures are illustrated in Figure 3.12.

Figure 3.12 Adhesion test.



To pass the requirement, the lubricant shall not lift to expose any bare metal surface, nor shall it soften, lift, blister, crack or peel. This same procedure is used to determine fluid resistance after the panels have been immersed in the fluids for 24-hours. A five-gallon

quantity of formulation A2200-69A was prepared for the evaluations and designated A2200-91. The coated panels were mounted upright in small tanks so that only the bottom half of the panel was submerged in the fluid. After immersion, each panel was rinsed with acetone and then left supported upright for one hour to allow the residual solvent to evaporate. Each test panel was then subject to the adhesion test described by the sequence of photographs shown in Figure 3.11.

Figure 3.13 Coated test specimens drying after immersion in jet fuel and gun cleaning fluid.



Panels coated with formulation A2200-91 were examined for fluid resistance and passed the requirements. Figures 3.12 and 3.13 are photographs of panels after immersion in the two most aggressive fluids, followed by required adhesion testing. Panels immersed in

water, de-icing fluid, mineral oil, hydraulic fluid and 1,1,1-trichloroethane also met the performance requirement.

Figure 3.14 Adhesion test results of after cleaning fluid immersion.

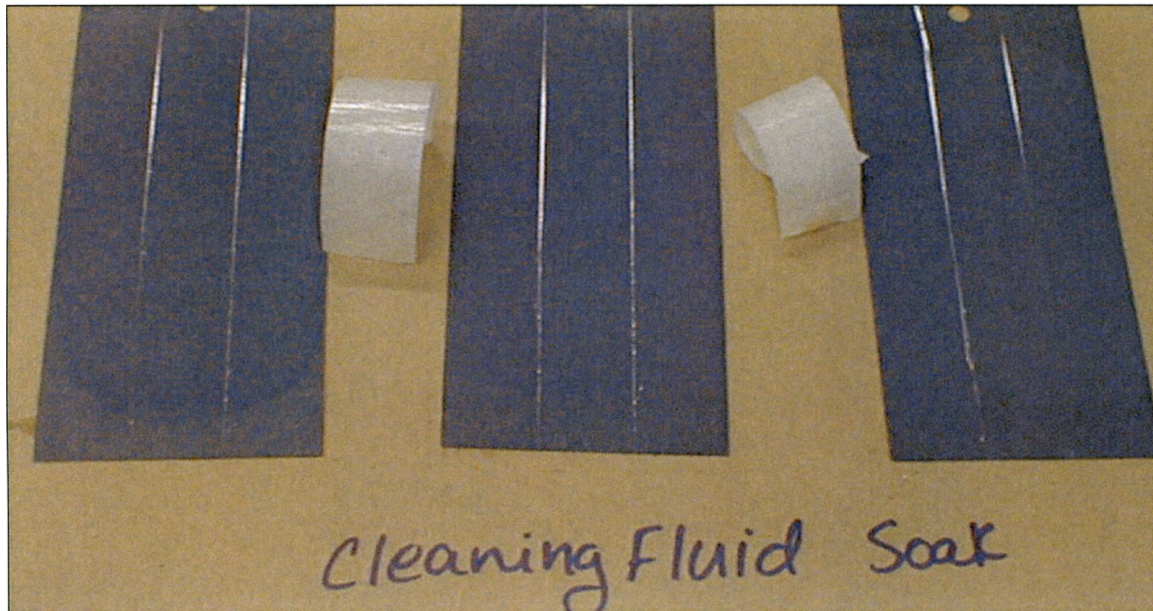
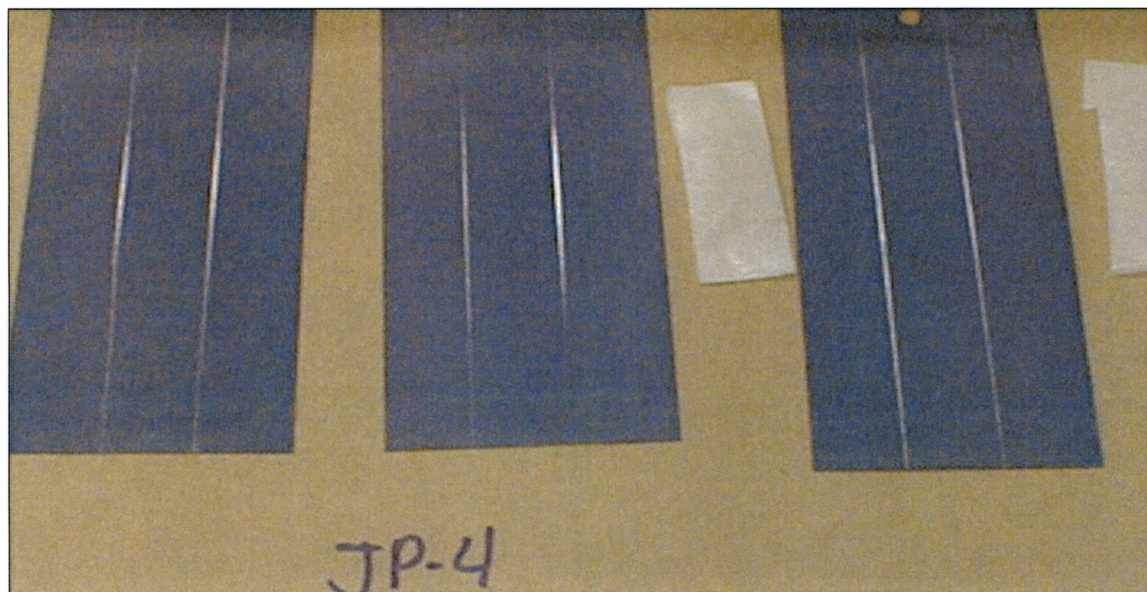


Figure 3.15 Adhesion test results after jet fuel immersion.



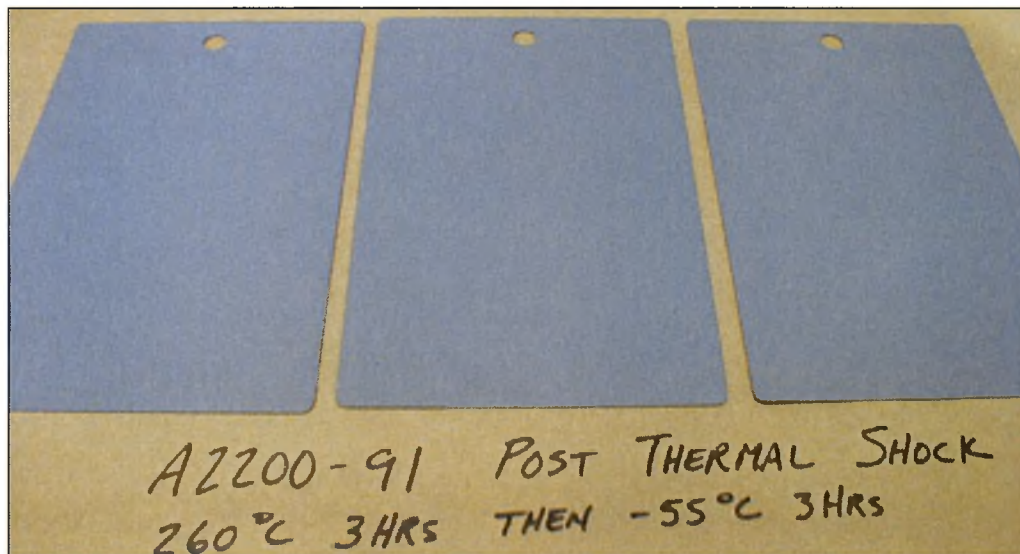
3.8 Thermal Shock Sensitivity

Lubricant formulation A2290-91 was subjected to thermal shock temperature cycles between 260 °C and negative 55 °C, following ASTM D2511 procedures.² Coated panels were held at elevated temperature for three hours then rapidly transferred to depressed temperature and equilibrated for three hours. The cycle simulates aerospace applications where aircraft in hot desert environments rapidly ascend to altitudes with extremely low temperature. The chambers used to perform this test are shown in Figure 3.14. The lubricant shown in Figure 3.15 readily passed the test, without loss of adhesion, spalling, cracking or other coating failures.



Figure 3.16 Laboratory arrangement for thermal shock treatment: The left chamber is set at 260 °C and the right at negative 55 °C.

Figure 3.17 Formulation A2200-91 after thermal shock between 260 °C and negative 55 °C



3.9 Aluminum Corrosion Resistance

Procedures listed in ASTM D 2649 were followed to evaluate the aluminum corrosion resistance of the lubricant. Aluminum panels specified in MIL-L-23398 were coated with the lubricant, cured for seven days at room temperature, and then placed into a salt fog cabinet for 100 hours. After exposure the panels were visually inspected and found to be free of corrosion.

3.10 Sulfurous Acid Salt Spray

The sulfurous acid salt spray analysis was conducted by a commercial testing lab equipped to perform the test per MIL-L-23398 specifications. Coated metal panels were subjected to prescribed sulfurous acid salt spray cycling. After exposure the panels were visually examined and found to be free of corrosion.

3.11 Storage Stability

One year product storage stability at standard room temperature and humidity conditions (25 °C and 50% relative humidity) is required by MIL-L-23398. After aging the sample is required to pass sulfurous acid salt spray resistance and endurance life. A one-quart sample of formulation A2200-91 was sent to a commercial laboratory equipped to conduct the analysis. The molybdenum pigment settled during storage but readily dispersed back into solution. Re-evaluation of the performance requirements yielded successful results, meeting storage stability requirements.

CHAPTER 4

DESIGN OF EXPERIMENTS

4.1 Designation of Factors

The goal of the formulation development work was to identify the minimum number of coating components necessary to achieve maximum endurance life, minimum corrosion, and maximum in-can, shelf stability. Once these components were identified, a systematic experimental design was constructed using Design Expert. A mixture design was used with three factors. These were the concentrations of molybdenum disulfide and resin, and then the relative concentration of all other components as a block. This block contained water, coalescing agents, dispersing aids, and de-foamers each in the same relative concentration to one another for each of the factor levels in the experiment. The design is summarized in Table 4-1 which also lists the measured responses for three performance parameters of high interest for this developmental material. The series of fourteen experiments are listed in the standard order of the design. They were randomized and assigned a run order number to reduce bias.

Table 4.1 Optimal mixture design over three factors with three responses shown.

Standard Order	Run Order	MoS ₂ (%)	Resin (%)	Remaining Components (%)	Endurance Life (min)	Corrosion (1=Low)	In-Can Stability (1=Pass)
1	2	25.00	15.00	60.00	266	3	1
2	12	25.00	5.00	70.00	21	5	1
3	1	10.00	20.00	70.00	31	2	1
4	9	5.00	35.00	60.00	3	1	1
5	13	5.00	15.00	80.00	9	3	1
6	4	15.00	5.00	80.00	17	5	1
7	11	15.00	25.00	60.00	68	3	1
8	8	17.50	10.00	72.50	0	5	0
9	7	10.00	15.00	75.00	21	3	0
10	3	15.00	20.00	65.00	42	2	1
11	6	5.00	35.00	60.00	2	1	1
12	14	15.00	5.00	80.00	132	4	1
13	10	5.00	15.00	80.00	0	3	0
14	5	25.00	15.00	60.00	245	4	1

The run order was used to proceed with sample formulations followed by testing for endurance life, salt fog corrosion resistance, and product stability.

4.2 Designation of Responses

Endurance life was determined on a continuous scale based upon the number of minutes to failure, which typically occurred when the torque increased by ten inch-pounds over the running baseline (typically 2-4 inch-pounds). The corrosion scale was developed by laying the sample plates side-by-side on an increasing scale of corrosion based upon visual inspection, and then artificially subdividing the total range of corrosion observed into five groups. No identifying markers were visible when this scale was designed. On this scale a ranking of one represents a sample with no visible corrosion, and a ranking of five is for a completely corroded sample. In-can stability was rated zero or one (fail or pass, respectively) and this was assessed by visual inspection for increased

viscosity or gel over a one-week period during which the sample was stored at room temperature. After reflection and a review of the response surface, it was decided that no further analysis of in-can stability could be performed with the data obtained in this experimental design, since there was insufficient resolution in the scale used to assess it.

Four pairs of the experimental cells in Table 4.1 were replicates of the formulation. These are built into the design to assess the inherent variability of the formulation and the tests used to obtain the responses. These are summarized in Table 4.2, and listed by Run Order Number. Also shown in the table are test results and the relative amounts of molybdenum disulfide and resin.

From these data it can be seen that the relative variation in endurance life increased for lower levels of molybdenum disulfide, but the absolute variation tended to decrease in magnitude. Variation in corrosion level was generally low for the four pair of replicates. Higher levels of lubricant and resin increased endurance life and decreased corrosion. Correlation coefficients were approximately 90% for these relationships (see R^2 values in Figures 4.1 & 4.2).

Table 4.2 Analysis of four replicate pairs from the mixture design.

Run Order Number	Endurance Life	MoS ₂ (%)	Corrosion	Resin (%)
2	266	25	3	15
5	245		4	
6	2	5	1	35
9	3		1	
4	17	15	5	5
14	132		4	
10	0	5	3	15
13	9		3	

For clarity these data are plotted in Figures 4.1 and 4.2 below. A least squares linear fit to the data is also shown in each figure, together with the respective correlation coefficients. In spite of the apparent fluctuation in the data spread, the linear fit in Figure 4.1 explains 88% of the variation, while the fit in Figure 4.2 explains 91%. At this point the low reading at 15% MoS₂ was suspected to be anomalous, but was not excluded from the series, since it could not be explained by any substantive or reasonable alterations in the procedure.

Figure 4.1 Plot of endurance life vs. MoS₂ concentration.

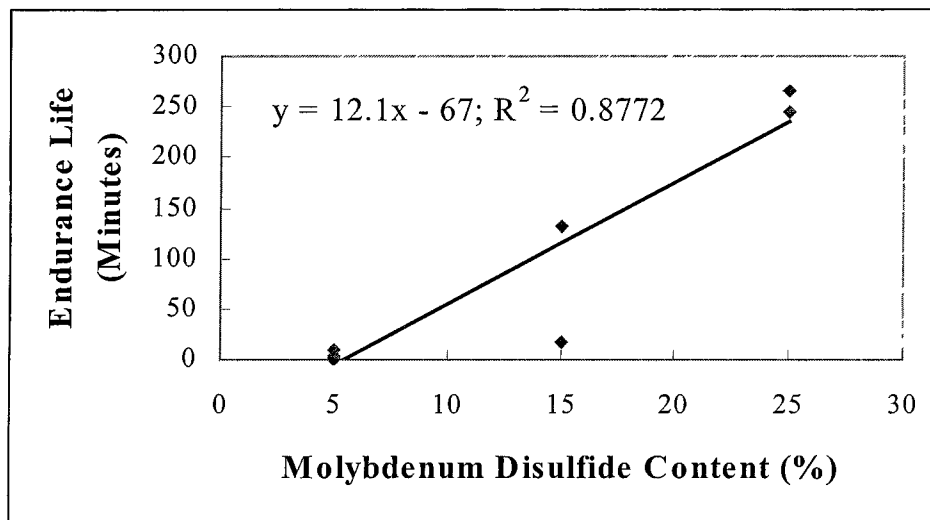


Figure 4.2 Plot of corrosion level versus resin content.

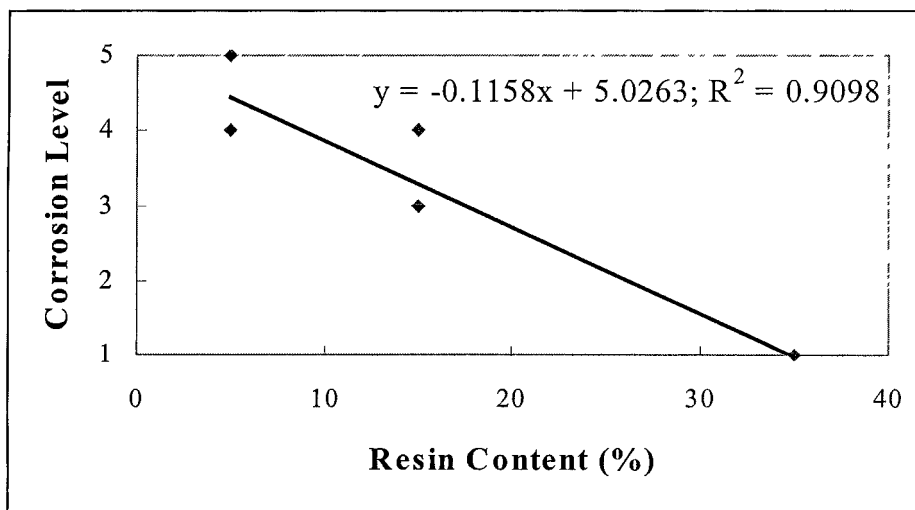
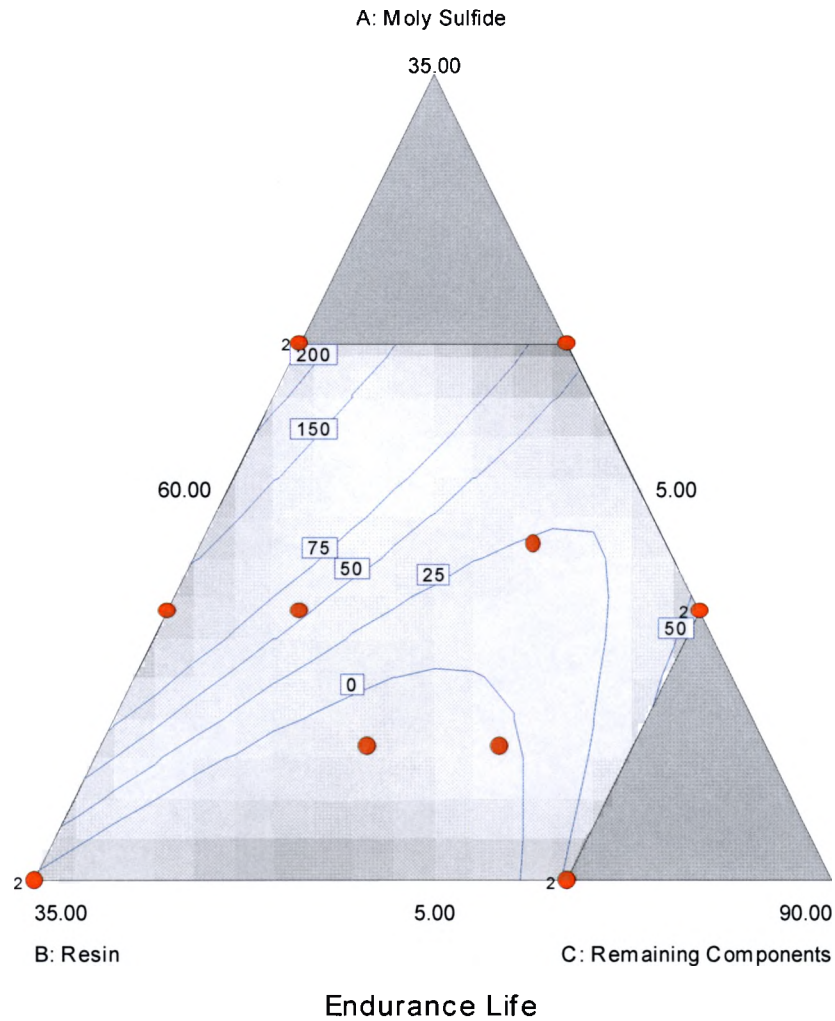


Figure 4.3 Response surface contour diagram of endurance life over the three factors, MoS₂, resin and remaining components.



The plot suggests increasing relative MoS₂ content increases endurance life. The final equation in terms of the actual model components was found to be given by:

Corrosion Resistance =

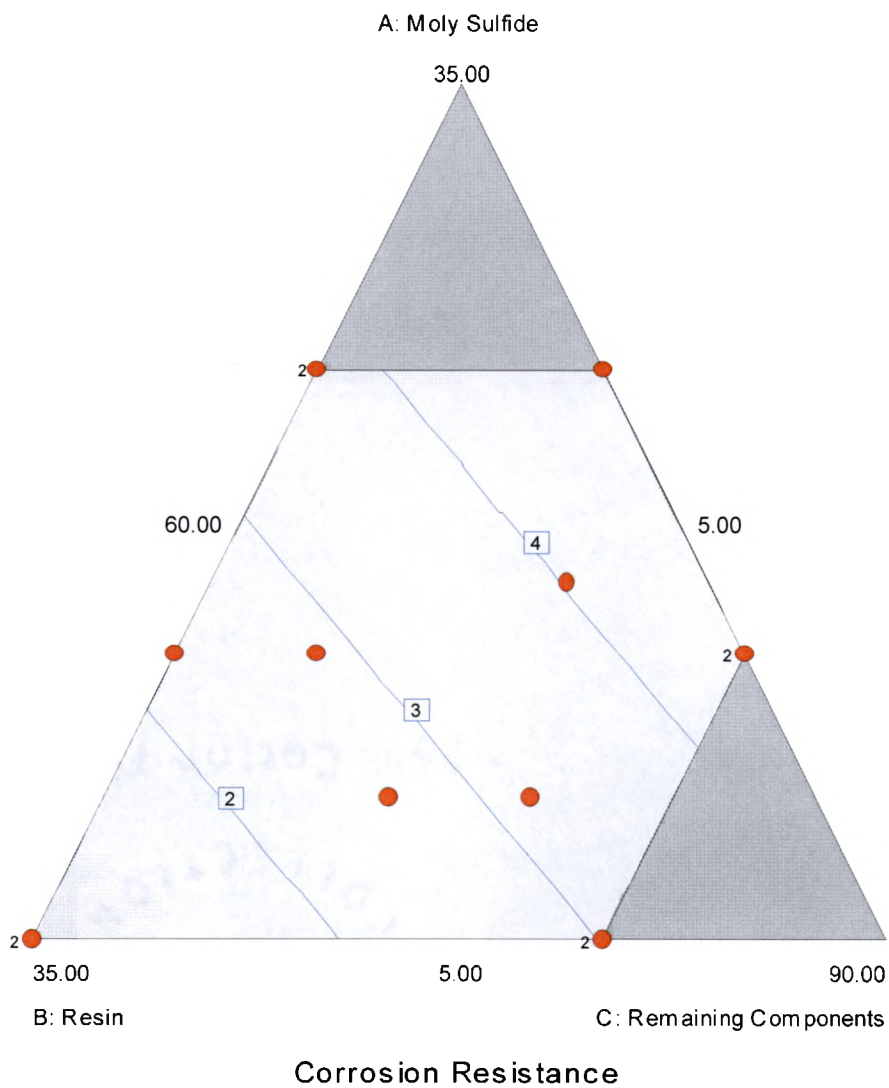
$$0.08 * \text{Moly Sulfide} \\ -0.06 * \text{Resin} \\ 0.04 * \text{Remaining Components}$$

The signs and relative magnitudes of the coefficients in this equation are telling. Bear in mind that the equation fit the data to a “negative” scale. A value of one indicated no corrosion and a value of five indicated the highest level of corrosion. In other words, the negative resin coefficient meant increasing resin content would decrease corrosion.

Conversely, increasing the molybdenum disulfide would increase corrosion, as would the block of remaining components. It is not to suggest that the molybdenum disulfide or remaining components were active corrosion promoters. Rather, they competed with the resin, and possibly interfered with its ability to form a film of sufficient integrity to block corrosive agents from the substrate surface.

The analysis at this point suggested that a composition represented by the lower left corner of the diagrams in Figures 4.3 and 4.4, was near the correct compromise to minimize corrosion and achieve an endurance life acceptable for MIL-L-23398.

Figure 4.4 Response surface contour diagram of corrosion over the three factors, MoS₂, resin and remaining components.

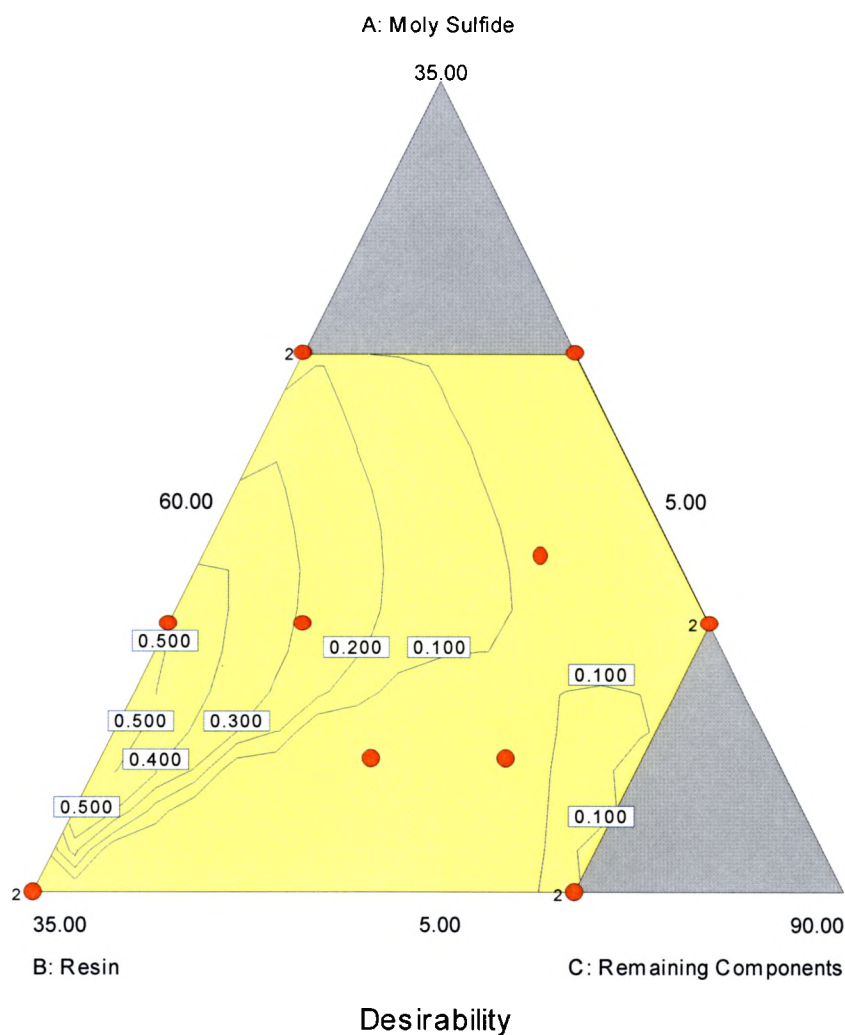


4.3 Optimization

The next step in the analysis was to perform an optimization of the compositions to unambiguously determine the compositional region of choice. This analysis incorporated weighting factors for an upper limit for endurance life and a lower limit for corrosion to

emphasize the relative importance of these two opposing requirements. A contour diagram of a desirability plot is shown in Figure 4.5. This figure suggests that the experimental formulation is close to an optimum composition at the edge of the diagram, and that, perhaps, a better compromise would be found in the region to the left of that covered by the design space in Figure 4.5.

Figure 4.5 Optimization results showing contour diagram of an overall desirability analysis.



CHAPTER 5

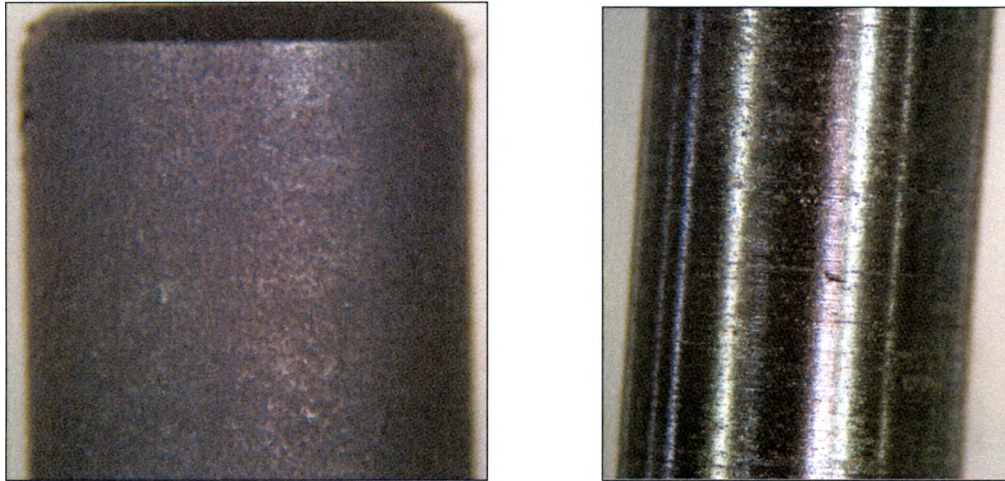
SPECTROSCOPIC ANALYSIS OF THE DRY FILM LUBRICANT

This chapter contains a description of spectroscopic techniques, instruments, images and spectra used to characterize the lubricant. Surface evaluations of the lubricant were conducted after various stages of endurance life wear. Studies ranged from macroscopic (optical) to atomic (XPS and AFM).

5.1 Optical Microscopy

Optical microscopy was suitable for initial lubricant characterization due to ease of use, low cost and ready availability. A research grade stereomicroscope captured magnified 3-dimensional images of pin specimens after various stages of wear. Specimen 1 was an unworn, pristine pin used as a control. Specimen 2 was subjected to reduced load pressures during break-in, while Specimen 3 was worn for 30-minutes with 1000-pound applied load. Specimen 4 was worn under maximum load until lubricant failure. Figure 5.1 is a photograph of Specimens 1 (left) and 2 (right).

Figure 5.1 Optical microscopy of the surface of pin specimens after various stages of wear.



Close inspection of Specimen 2 in Figure 4.1 revealed a defect on the pin surface formed during the break-in period. Figure 5.2 is a more detailed view of the defect.

Figure 5.2 Defect on the surface of Specimen 2.



Optical microscopy revealed the burnished lubricant on Specimen 3 had a surface morphology that, upon closer inspection, was not homogenous. Figure 5.3 is a photograph of Specimen 3. The top section of the pin, after 30-minutes of extremem pressure wear, had a defined, macroscopic topography while the lower section appeared smooth and continuous.

Figure 5.3 Optical microscopy of Specimen 3.



Specimen 4 was worn under extreme pressure conditions until lubricant failure. The photograph in Figure 5.4 shows distinct wear scars on the upper and lower sections. The lower scar on the specimen was deeper and more pronounced than the one above. The deep scar was the point of lubricant failure that caused an abrupt torque increase detected by the Falex machine.

Figure 5.4 Optical microscopy of Specimen 4.



Optical microscopy was able to detect macroscopic defects on the coating surface that formed during the lubricant break-in period. It also showed the surface morphology of the burnished coating of Specimen 3. Finally, deep wear scars at the point of lubricant failure on Specimen 4 were closely inspected using microscopic analysis.

5.2 X-ray Photoelectron Spectroscopy

X-ray photoelectron spectroscopy (XPS) was used to characterize inorganic and organic solid materials present on the lubricant surface after various stages of wear.⁴¹ The lubricant surface was excited with Al monochromatic x-rays (1486.6 eV) and the photoelectrons ejected from the surface were energy analyzed. A low resolution surface scan analysis was used to identify the elements present (except H and He) and establish a concentration table in units of atom %. High resolution analysis of individual photoelectron signals was used to identify chemical bonding and oxidation states.

Four endurance life pin specimens were coated with lubricant A2200-91, subjected to various levels of wear and analyzed. Specimen 1 was used as a control. It was pristine and not subjected to wear. Specimen 2 subjected to mild “break-in” period load pressure and minor wear. Specimen 3 was worn under the peak 1000-pound applied load for thirty minutes. Specimen 4 was worn under extreme pressure for 63 minutes, essentially to failure. The goal of this analysis was to determine compositional changes on the surfaces of the pins.

For the analysis, each specimen was placed within a depressed well of a solid stainless steel sample holder and held by metal clips. They were orientated such that the analysis spot was between two scribe marks located on the outer circumference of the

length of the pin. The marks were made to ensure that XPS measurements and subsequent AFM and FT-IR measurements would be made in the same location. All sample holders were evacuated in the preparation chamber prior to insertion into the analytical chamber for XPS measurements.

The surface of each sample was measured by a low resolution XPS survey scan to determine which elements were present. Medium resolution spectra of each element (from the prior survey) were used to determine each element's oxidation state or chemical bonding environment. The analytical conditions for the XPS experiments are listed in Table 5.1. A low energy electron gun was used for charge neutralization. Specimen 1 required the most charging, which was not unexpected for a sample containing fluorocarbons.

The quantification of the elements was accomplished by using the atomic sensitivity factors from Physical Electronics' MultiPak software (V6.1A). The approximate escape depth ($3\lambda \sin\theta$) of the carbon electron (C 1s) was $\sim 50\text{\AA}$.

Table 5.1 Analytical conditions of the XPS experiments.

Instrument	Physical Electronics 5500 ESCA/XPS
X-ray Source	Standard Aluminum (1486.6 eV)
Source power	400 watts
Aperture	Slit: 4x10 mm
Takeoff Angle*	45°
Charge Correction	C-C,H in C 1s spectra at 284.8 eV
Charge Compensation	Low energy electrons

* Takeoff angle is defined as the angle between the surface plane and the electron analyzer lens.

The XPS survey spectra in Figures 5.5 – 5.8 are shown as color plots of electron counts versus binding energy (eV). The main photoelectron peaks (*i.e.*, O 1s) are labeled.

The medium resolution spectra in Figures 5.9 – 5.12 are also shown as color plots of electron counts *versus* binding energy (eV). Several of the medium resolution spectra were fit with a minimum number of peaks and assignments are based upon comparisons to at least two reference sources.^{45, 46}

Figure 5.5 Survey spectra of unworn, pristine specimen.

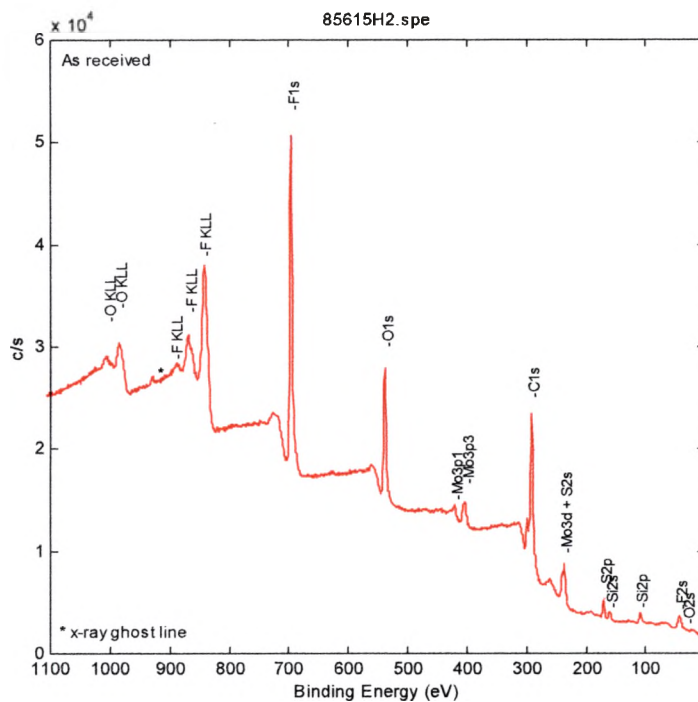


Figure 5.6 Survey spectra of endurance life specimen subjected to break-in load.

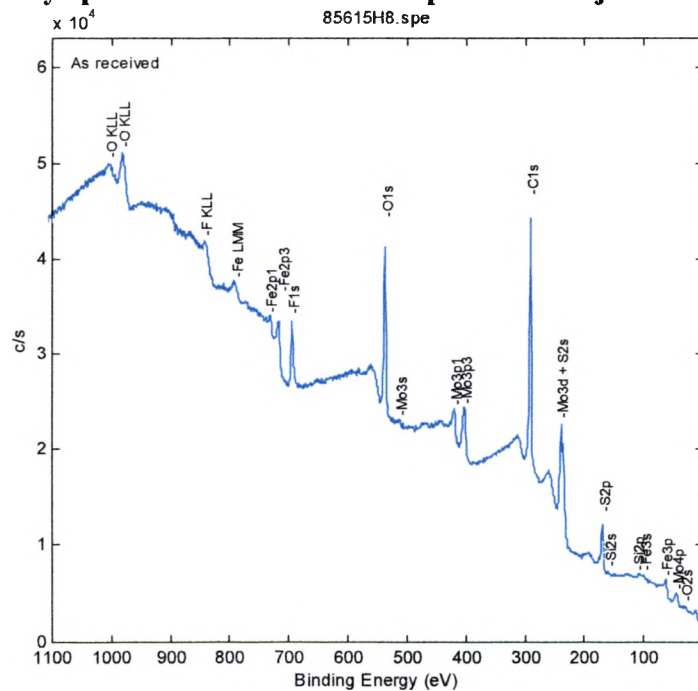


Figure 5.7 Survey spectra of endurance life specimen taken mid point of endurance life.

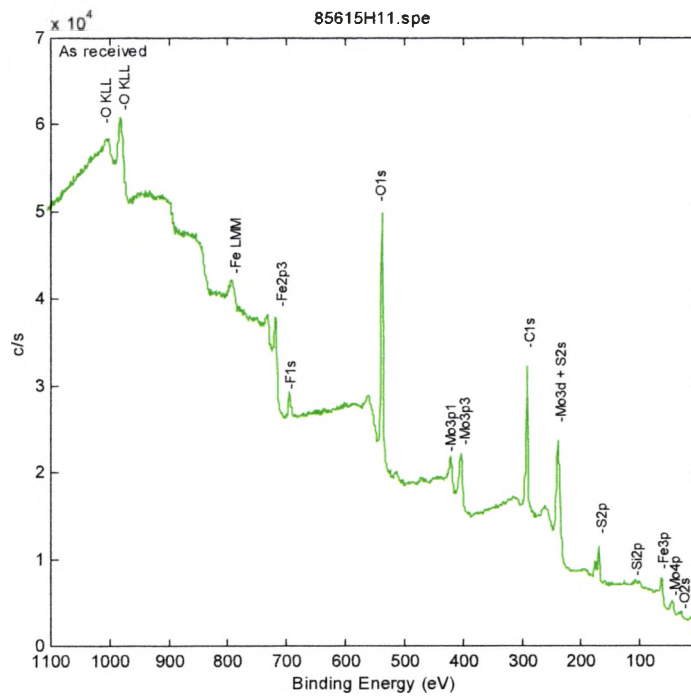


Figure 5.8 Survey spectra of endurance life specimen taken at coating wear through.

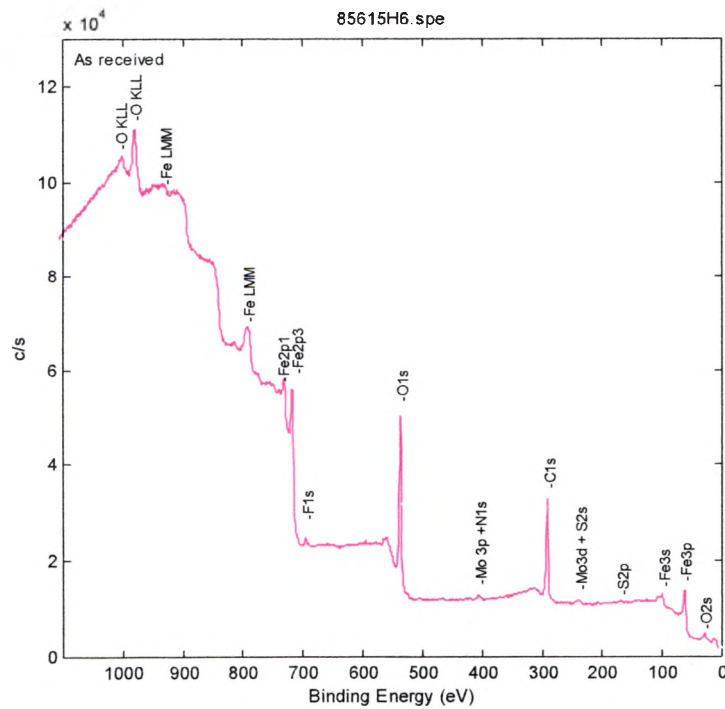


Figure 5.9 Medium resolution spectra of the unworn test standard.

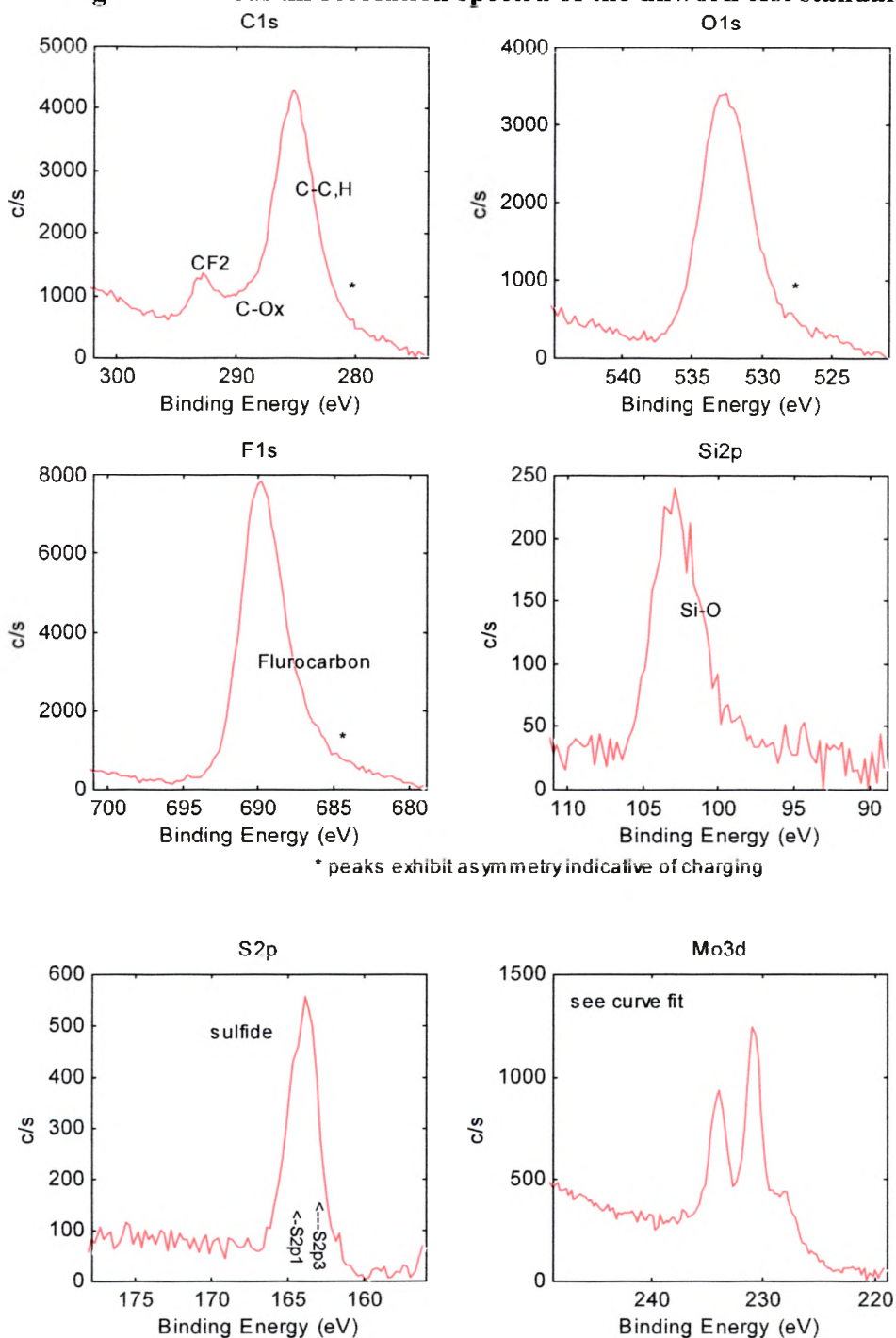


Figure 5.10 Medium resolution spectra specimen 2, subjected to mild break-in endurance life conditions.

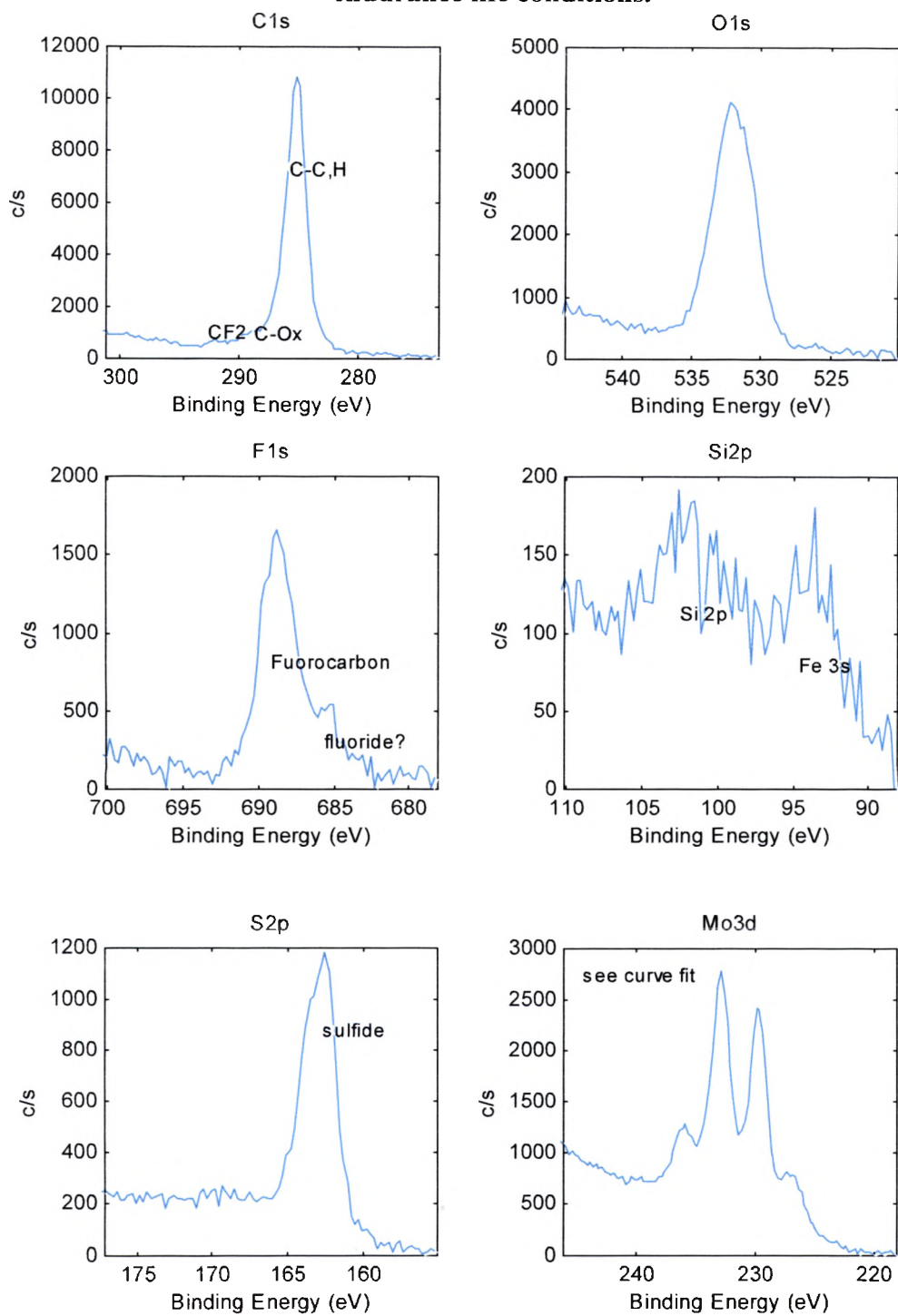


Figure 5.11 Medium resolution spectra of specimen 3, subjected to 30-minutes extreme pressure endurance life.

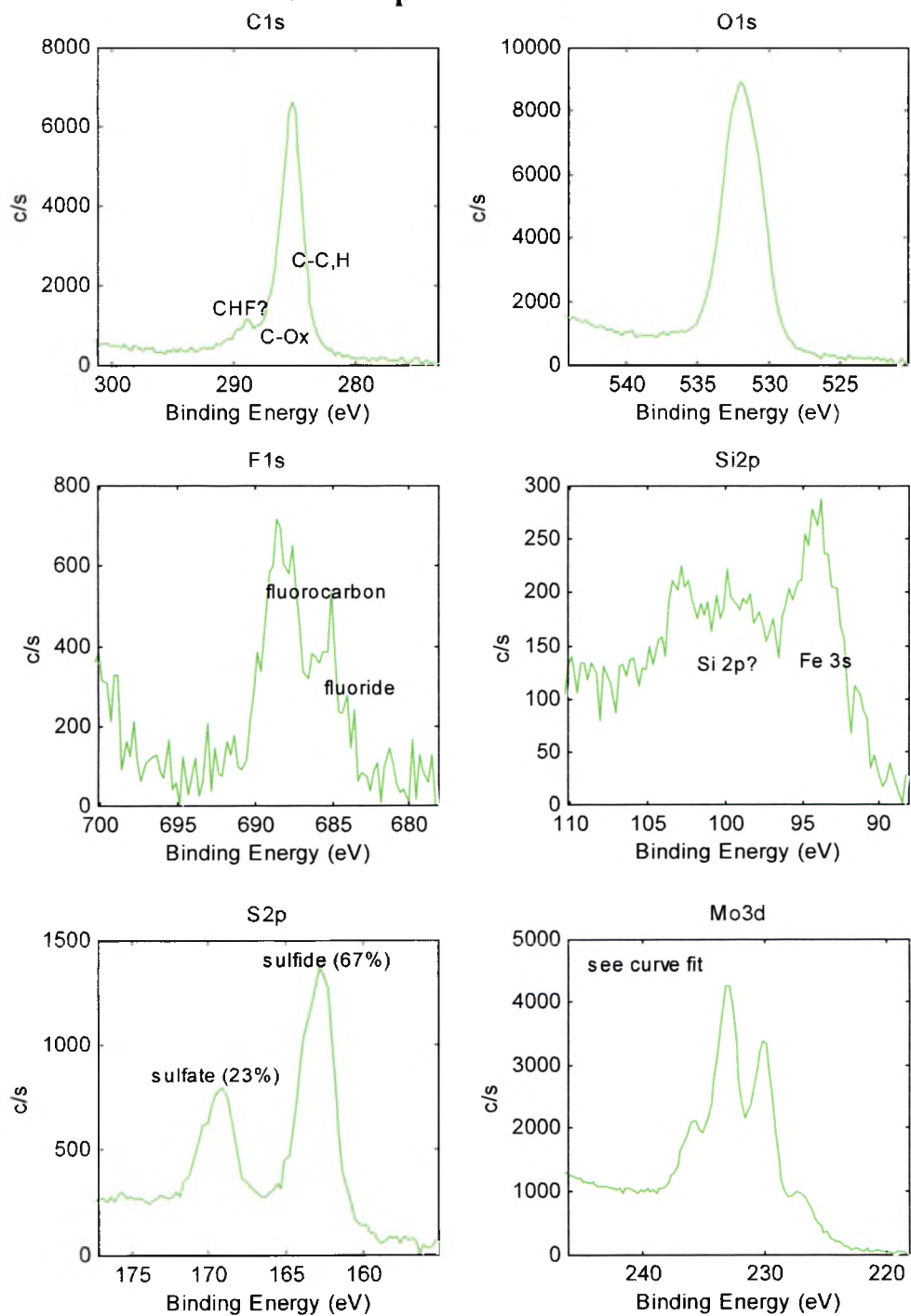
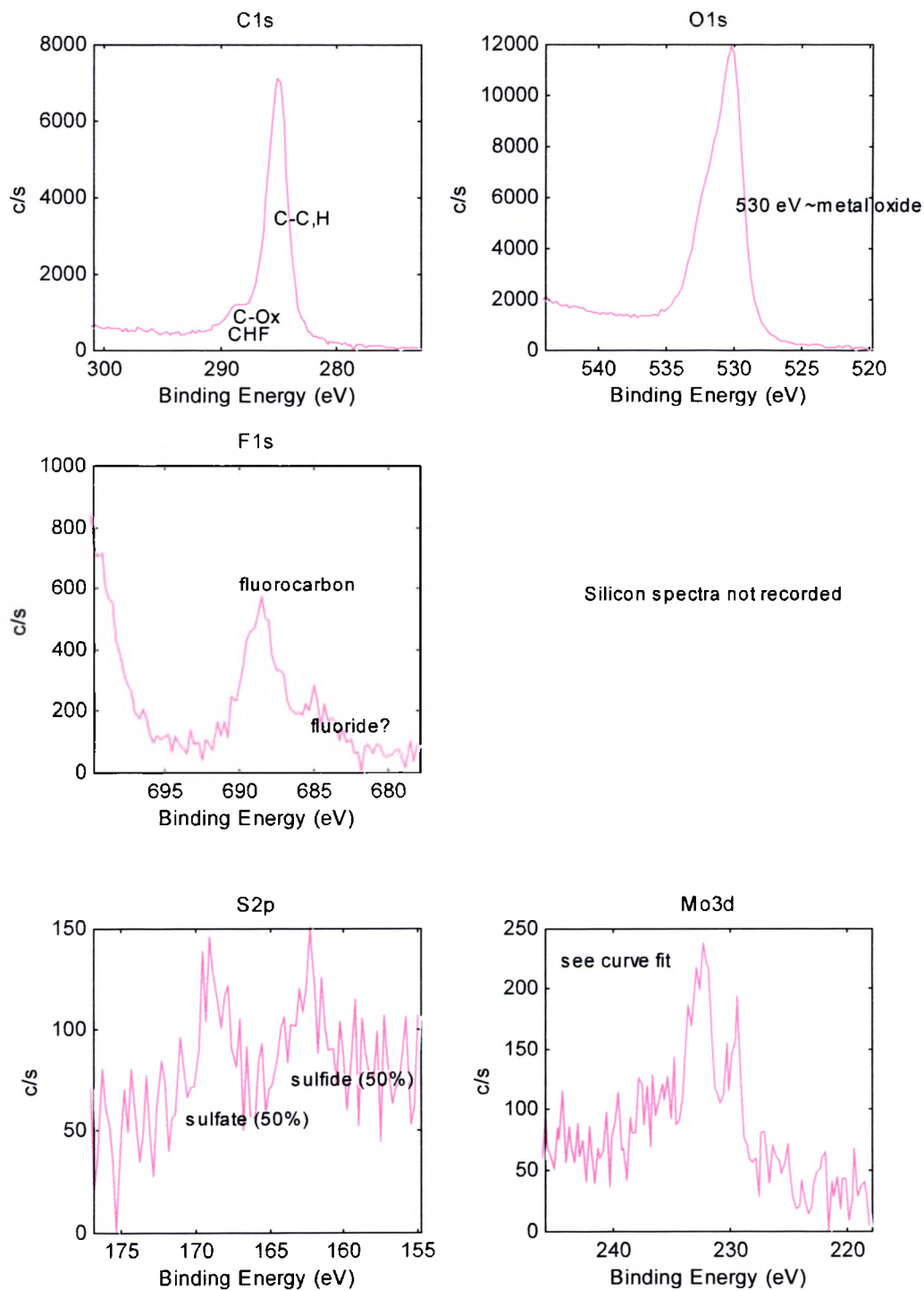


Figure 5.12 Medium resolution spectra of specimen 4, subjected extreme pressure endurance life until lubricant failure.



Survey Spectra Results

Elements identified on the outer circumference of each specimen were carbon, oxygen, fluorine, silicon, sulfur and molybdenum. Iron was detected on specimens 2, 3, and 4. Low concentrations of nitrogen may be present, but the nitrogen signal (N 1s) could not be resolved from the stronger molybdenum signal (Mo 3p3).

Medium Resolution Spectra Results

The semi-quantitative results of the analysis from medium resolution spectra are summarized in Table 5.2. In this case, the area under each peak after background subtraction was used to calculate concentration. Neither H nor He can be detected by XPS and all concentrations are normalized to 100%.

The results suggest that the surface of the dry lubricant on Specimen 1 was composed of a mixture of carbon oxides (C-O_x), fluorocarbons (CF₂, CHF) and molybdenum sulfide (MoS_x). It is not possible to determine if the presence of hydrocarbons (C-C,H) is from the lubricant and/or adventitious carbon found on all samples exposed to atmospheric conditions. The absence of a metal peak from the surface of Specimen 1 (*i.e.*, Fe) suggests that the lubricant thickness was > 100Å.

Several trends were observed in the data when comparing Specimen 1 (control sample) with the other specimens that were subject to pressure and wear.

Carbon

Carbon was found as a mixture of hydrocarbons (C-C,H at 284.8 eV) and carbon oxides (C-O_x at >286 eV) and fluorocarbons (CF₂ at 292 eV) on Specimen 1. In comparison,

carbon was found as hydrocarbons and carbon oxides on Specimens 2, 3, and 4. It is possible that there may be a different fluorocarbon (CHF) present on Specimens 3, 5, and 7, but it is not possible to separate it from carbon oxides (C=O, COO) at the same nominal binding energy (288-290 eV).

Oxygen

Oxygen was found on all samples, although it is not clear of the exact distribution since the O 1s peaks were very broad. However, it is likely that there are metal oxides/hydroxides near 529-530.5 eV (*i.e.*, FeO_x, MoO_x) and carbon oxides (C-O_x) and sulfates (SO₄²⁻) at ≥532 eV. The metal oxide component was most abundant on the surface of Specimen 4.

Fluorine

Fluorine was found as primarily as fluorocarbons (*i.e.*, CF₂) on Specimen 1 and then as mixture of fluorocarbons and inorganic fluorine (fluorides) on Specimens 2, 3, and 4.

Sulfur

Sulfur was found as a sulfide (S²⁻ at 162-163 eV) on Specimens 1 and 2 and then as a mixture of sulfides and sulfate (SO₄²⁻ at > 168 eV) on Specimens 3 and 4. The sulfur spectra (S 2p) were fit with one constraint; the area ratio of S 2p1 to

$$S\ 2p3 = 0.5.$$

Iron

Iron was detected as iron oxide (Fe 2p3 at >710 eV) on Specimens 2, 3, and 4.

Molybdenum

Molybdenum was found as molybdenum sulfide (Mo 3d5 at ~229.5 eV) on Specimen 1 and then as a mixture of molybdenum sulfides and molybdenum oxides (MoO_x, Mo 3d5 at ~232.5 eV) on Specimens 2, 3 and 4. The molybdenum spectra (Mo 3d) were fit with two constraints; the area ratio of Mo 3d3 to Mo 3d5 = 0.67 and the difference between Mo 3d3 and Mo 3d5 = 3.13 eV. Curve fitting these spectra also involved incorporating appropriate sulfur peaks (S 2s) to obtain the best fit to the raw data.

**Table 5.2 Concentration of Elements at the SURFACE
from XPS Medium Resolution Data[†]**

Atomic Concentration (%)

Sample	C	O	F	Si	S	Fe	Mo
Specimen 1	54.0	16.7	25.1	1.8	1.5	*nd	0.9
Specimen 2	70.5	16.1	4.6	0.4	3.7	2.3	2.6
Specimen 3	46.8	31.9	2.0	0.4	6.3	8.4	4.2
Specimen 4	42.4	34.4	0.9	<0.4	0.3	21.9	0.1

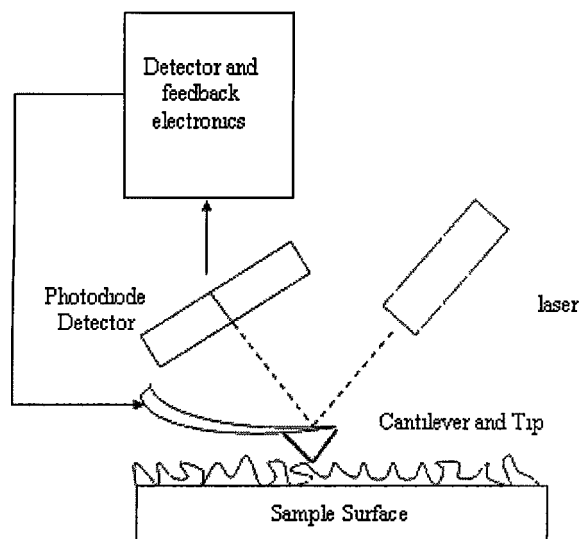
[†] XPS does not detect H (Hydrogen) and He (Helium) and all concentrations are normalized to 100%

*nd Element not detected. Detection limit is 0.1-0.5 atom % for most elements. Low concentrations of nitrogen can not be measured in the presence of molybdenum.

5.3 Atomic Force Microscopy

The surface of the Falex pin specimens were further evaluated by atomic force microscopy (AFM). This technique utilizes a scanned-proximity probe that measures local surface properties (height, optical absorption or magnetism) with a tip placed very close to the sample surface. To obtain an image the AFM scans the probe over the surface in a pattern of parallel lines that form the display of an image. The topography of the surface is determined by measuring attractive or repulsive forces between the silicon AFM tip and the sample surface. Figure 5.13 illustrates the principle.

Figure 5.13 The basic components of the AFM spectrometer and the optical beam deflection method.



The tip is attached to the end of a compliant cantilever. Attractive or repulsive forces between the tip and sample surface cause the cantilever to deflect toward or away from the sample. AFM has been identified as an important tool to study atomic-scale interactions such as friction, adhesion, lubrication and wear of surfaces in relative motion. ¹⁴

AFM images of the four specimens were obtained to measure surface roughness at the same locations previously examined by XPS. Specimen 1 was the unworn test standard, Specimen 2 was subjected to mild wear during break-in, Specimen 3 was worn for 30-minutes under extreme pressure and Specimen 4 was worn under extreme pressure until lubricant failure.

Image processing procedures involving auto-flattening, plane fitting and convolution were employed. The Digital Instruments Nanoscope III AFM/STM acquired and stored 3-dimensional representations of the lubricant surface in digital format.

Nanoscope III software was used to perform a roughness analysis of the AFM images. The product of analysis was a single color page reproducing the selected image in top view. To the right of the image is the "Image Statistics" box, which lists the calculated characteristics of the image.

One 20 μm x 20 μm area was imaged at the location between two markers on the outer circumference of each specimen. Top views of these areas are shown along with the roughness measurements in Figures 5.14 - 5.20. Topography differences of these images are presented in colors where green is low and red is high. The z ranges are noted on the prints. Perspective (3-D) views of these surfaces are also included with vertical exaggerations noted on the plots.

Figure 5.14 AFM roughness analysis of Specimen 1, the unworn test standard.

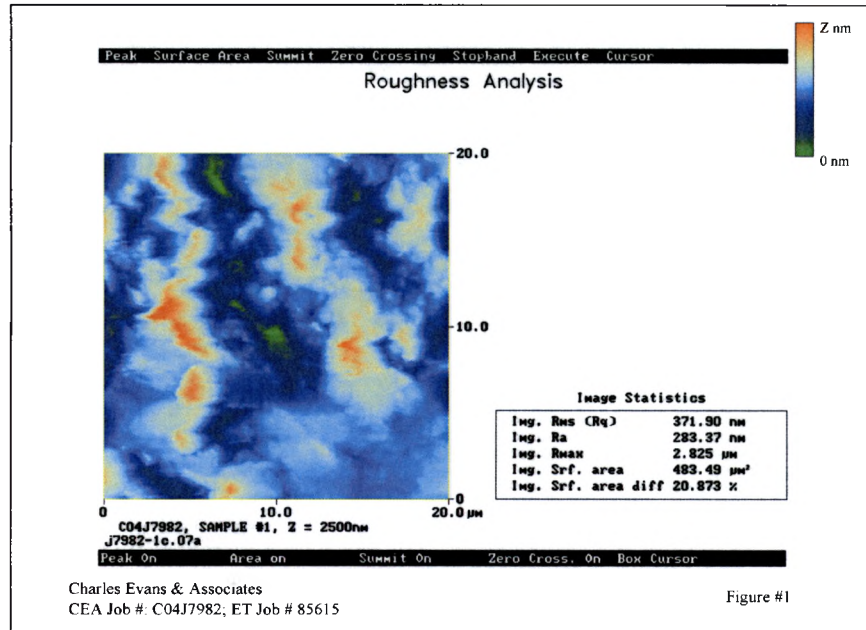


Figure 5.15 AFM 3-dimensional view of the unworn DFL coating.

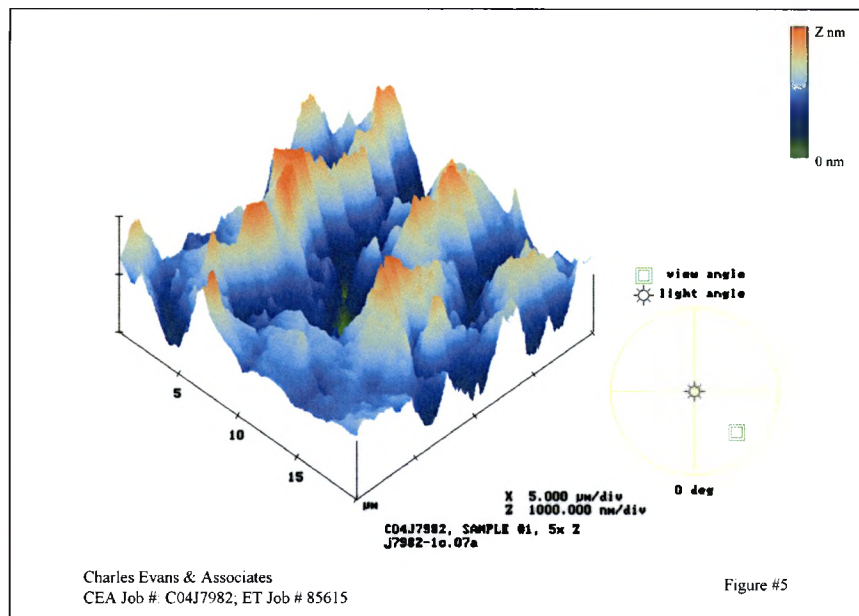


Figure 5.16 AFM roughness analysis of Specimen 2.

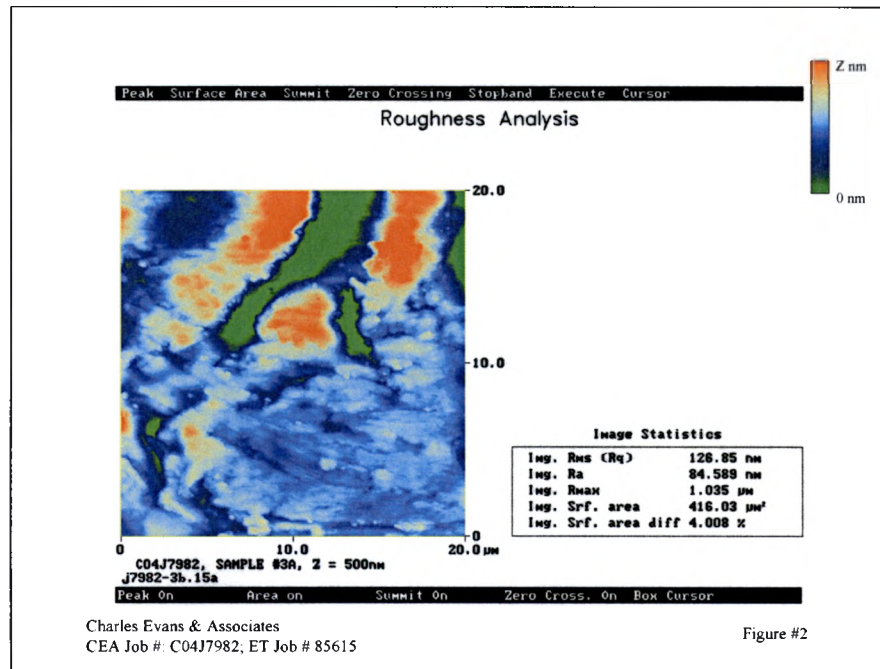


Figure 5.17 AFM 3-dimension view of Specimen 2.

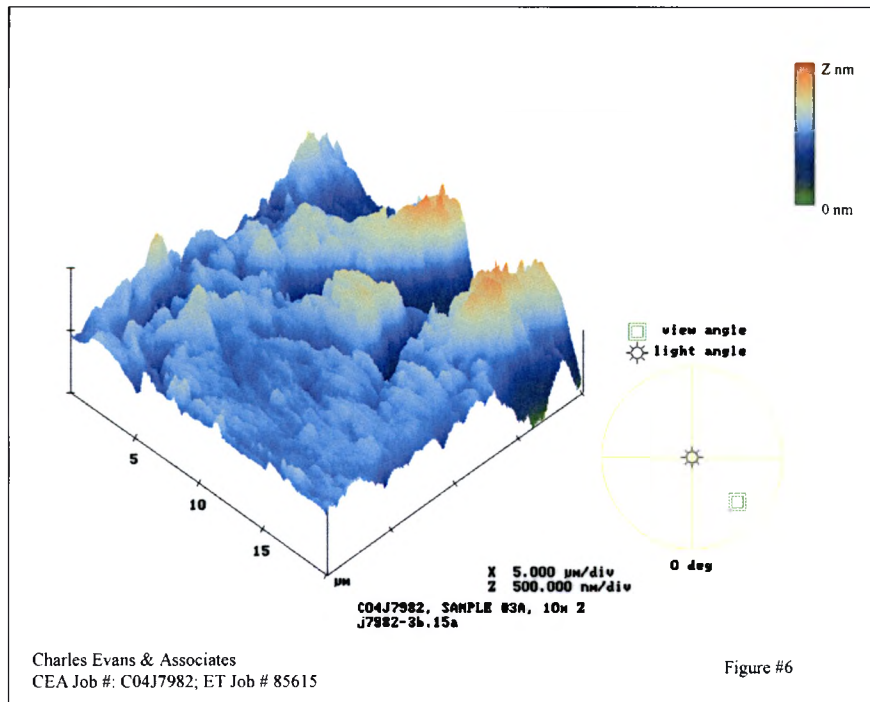


Figure 5.18 AFM analysis of Specimen 3.

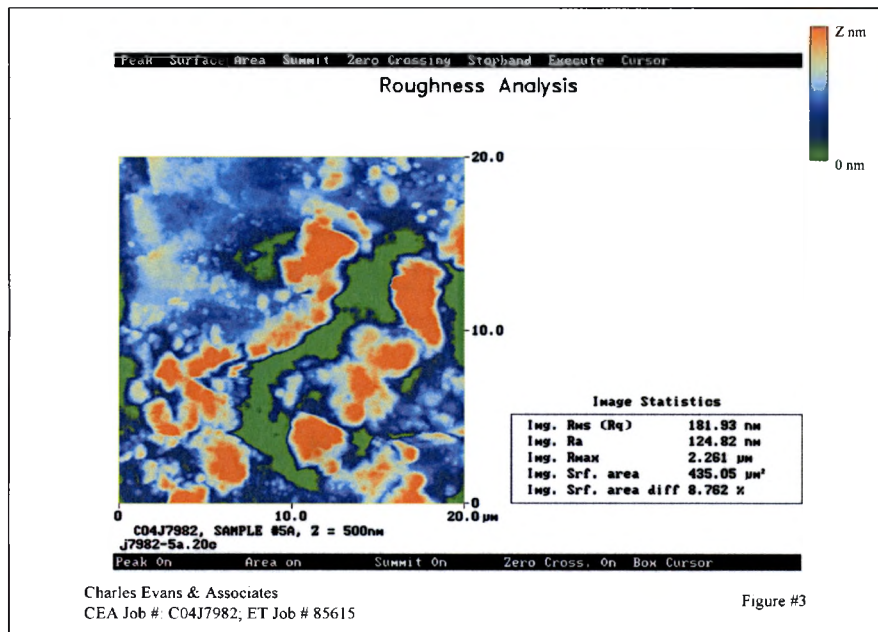


Figure 5.19 AFM 3-dimension view of Specimen 3.

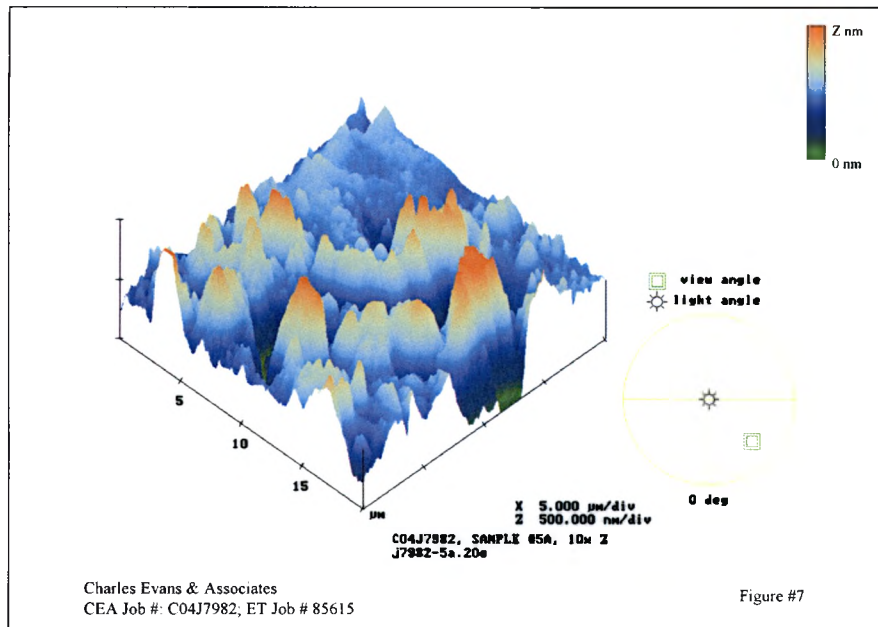


Figure 5.20 AFM analysis of Specimen 4.

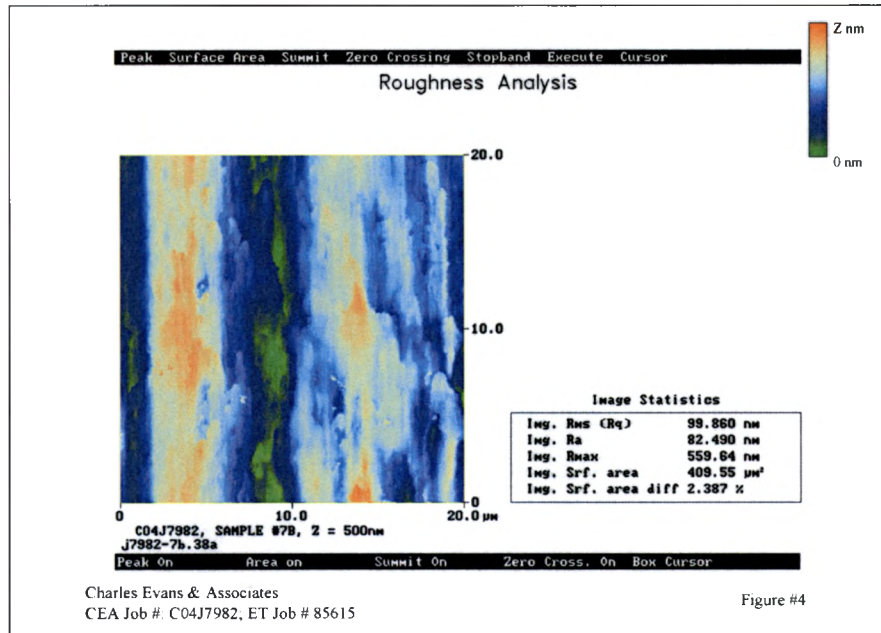
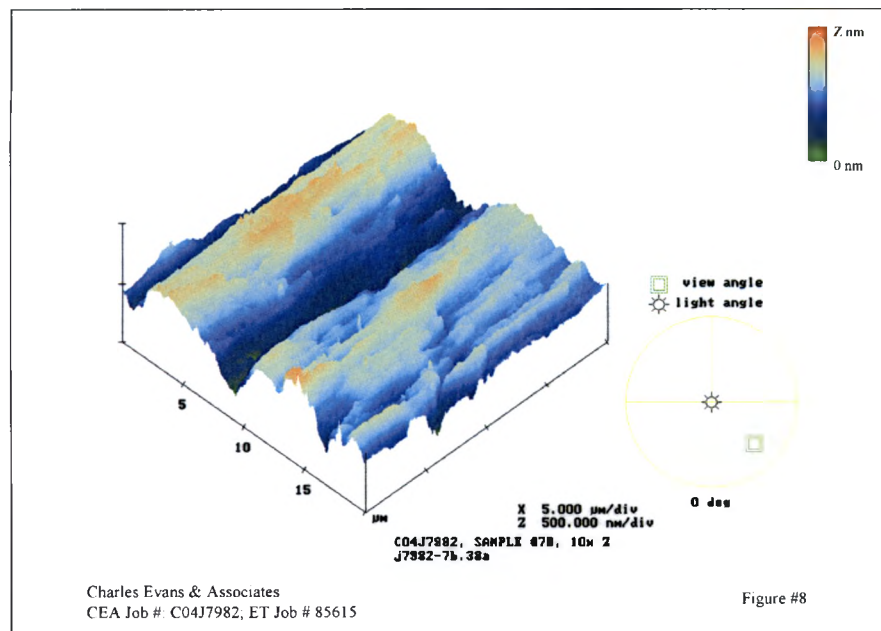


Figure 5.21 AFM 3-dimension view of Specimen 4.



The roughness analyses were performed and are expressed in: (1) Root-Mean-Square Roughness, RMS; (2) Mean Roughness, R_a ; and (3) Maximum Height (Peak-to-Valley), R_{max} . Results are summarized in Table 5.3, and a description of image statistics are presented in Table 5.4.

Table 5.3 AFM roughness results.

Sample I.D.	RMS (nm)	R_a (nm)	R_{max} (nm)
Specimen 1	371.90	283.37	2825.0
Specimen 2	126.85	84.59	1035.0
Specimen 3	181.93	124.82	2261.0
Specimen 4	99.86	82.49	559.64

Table 5.4 Description and explanation of the Image Statistics

Z Range (R_p)	Difference between the highest and lowest points in the image
Mean	Average of all of the Z values in the imaged area
RMS (R_q)	Standard deviation of the Z values (or RMS roughness) in the image. It is calculated according to the formula: $R_q = \sqrt{\{\Sigma(Z_i - Z_{avg})^2 / N\}}$ where Z_{avg} is the average Z value within the image; Z_i is the current value of Z; and N is the number of points in the image.
Mean roughness (R_a):	Mean value of the surface relative to the Center Plane and is calculated using the formula: $R_a = [1/(L_x L_y)] \int_0^{L_y} \int_0^{L_x} \{f(x,y)\} dx dy$ where $f(x,y)$ is the surface relative to the Center Plane, and L_x and L_y are the dimensions of the surface.

Max height (R_{max}):	Difference in height between the highest and lowest points of the surface relative to the Mean Plane.
Surface area:	Area of the 3-dimensional surface of the imaged area. It is calculated by taking the sum of the areas of the triangles formed by 3 adjacent data points throughout the image.
Mean Plane:	The image data has a minimum variance about this flat plane. It results from a first order least squares fit on the Z data.
Center Plane	A flat plane that is parallel to the Mean Plane.
Surface area diff.	Amount that the Surface area is in excess of the imaged area.

Presentation of the image statistics in Table 5.3 suggests that Specimen 1 is the roughest and Specimen 4 smoothest. In addition to being smoother, the morphology of Specimen 4 differs from that of the others. It appears to exist as smooth troughs and valleys running parallel to one another. The morphology of the other three specimens consists of randomly distributed peaks.

It is not surprising that the unworn coating is the roughest. MoS_2 particles are randomly oriented until rubbed or slightly worn under load. Tribologists frequently refer to this mild rubbing as “burnishing” of the solid lubricant. The process aligns the solid lubricant particles into a layered, lamellar orientation.

5.4 Fourier Transform Infrared Analysis (FTIR)

Infrared Spectroscopy probes characteristic molecular vibrations and is a useful analytical technique that provides specific information about chemical bonding and molecular structure of organic materials. It is based upon established vibrations and characteristic frequencies specific to bonds within organic molecules. When exposed to infrared radiation, a molecule selectively absorbs infrared frequencies that match those of its allowed vibration modes. Therefore, the infrared absorption spectrum of a material reveals which vibrations, and thus which functional groups, are present in its structure.

FTIR analysis was conducted to identify organic materials on the surfaces of the Falex pin specimens that were previously analyzed by XPS and AFM techniques. Metals are not active in the IR spectrum and not detected by this technique. Therefore, FTIR provided more specific information about the organic components of the lubricant as it was subjected to wear. The areas on the specimens analyzed were consistent with those of the other two techniques. Samples of the lubricant were physically removed from the surface of the pin specimens. FTIR was the last spectroscopic technique performed due to the destructive nature of the sample gathering technique.

Figure 5.22 is a spectrum of Specimen 1, the unworn lubricant standard. The strong absorption bands at 1226 and 1158 reciprocal centimeters (cm^{-1}) indicate the presence of PTFE. A strong signal centered at 2934 cm^{-1} is

attributable to the urethane polymer and perhaps the added surfactant (Envirogen AE-01). Absence of bands above 3000 cm^{-1} confirms the aliphatic nature of the urethane resin. In addition, absence of broad OH-stretch bands above 3000 cm^{-1} also suggest that the polyol used to make the urethane has been consumed, and the glycol ether coalescent aids evaporated from the lubricant surface. A strong band at 1726 cm^{-1} is consistent with the ester backbone of the polyester polyol used to synthesize the urethane polymer dispersion. The band at 1549 cm^{-1} is indicative of the organic acid salt used in the preparation of the urethane dispersion as discussed by Frisch.²² Figure 5.23 is a reference FTIR spectrum of neat PTFE.

Figure 5.22 FTIR spectrum of Specimen 1.

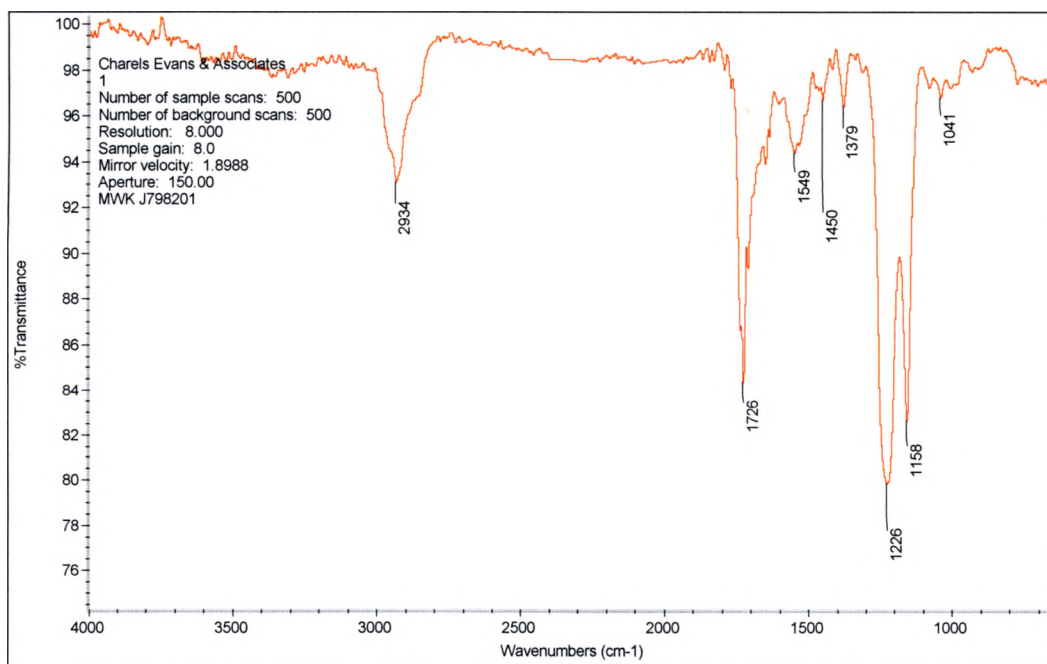
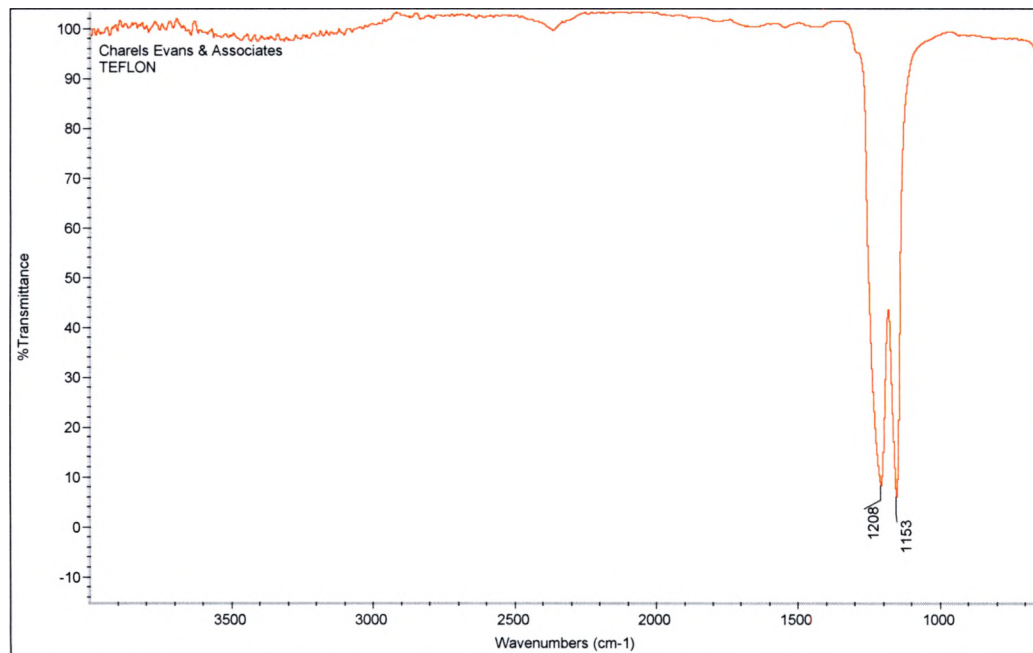


Figure 5.23 Reference spectrum of neat poly(tetrafluoroethylene).



Specimen 2 revealed a large reduction in percent transmittance, as seen on the vertical axis of the FTIR spectrum in Figure 5.24. This trend continued through the remainder of the series and suggests that organic content on the specimen surface rapidly diminished during wear. The ester, fluorocarbon and hydrocarbon bands remained, while a broad band centered at 3437 cm^{-1} that was not detected in Specimen 1 appeared after wear. The position and broadness of the peak suggests the presence of an alcohol or organic acid. It is possible that the glycol ether coalescent aids remained beneath the lubricant surface and were liberated during wear.

Figure 5.24 FTIR spectrum of Specimen 2, subjected to milder wear conditions during the break-in period.

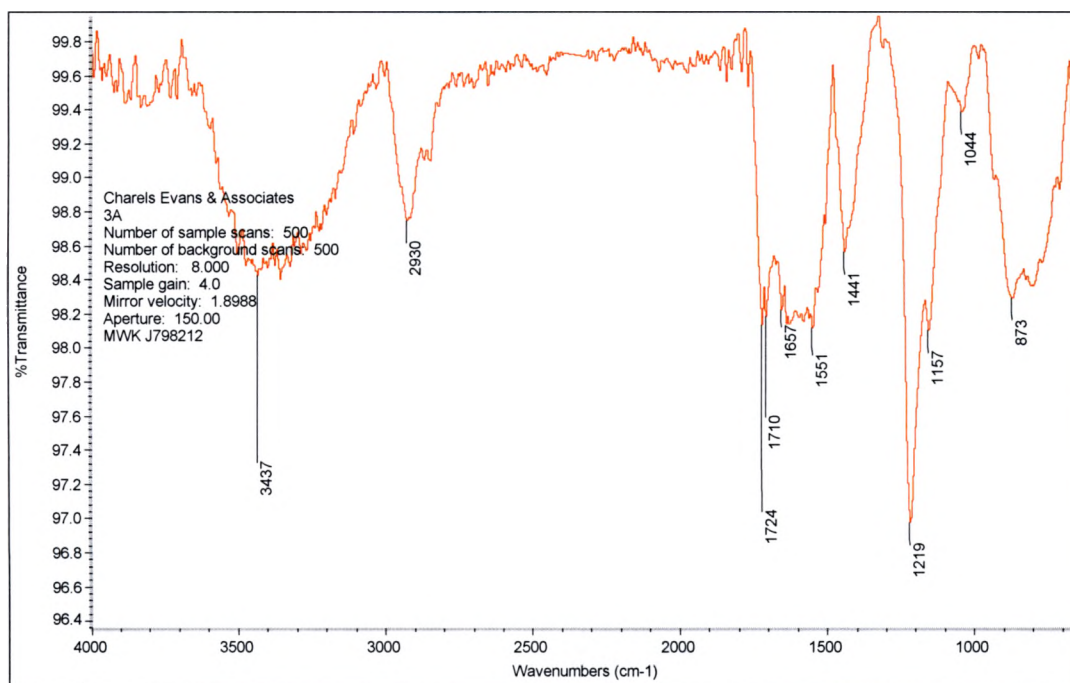
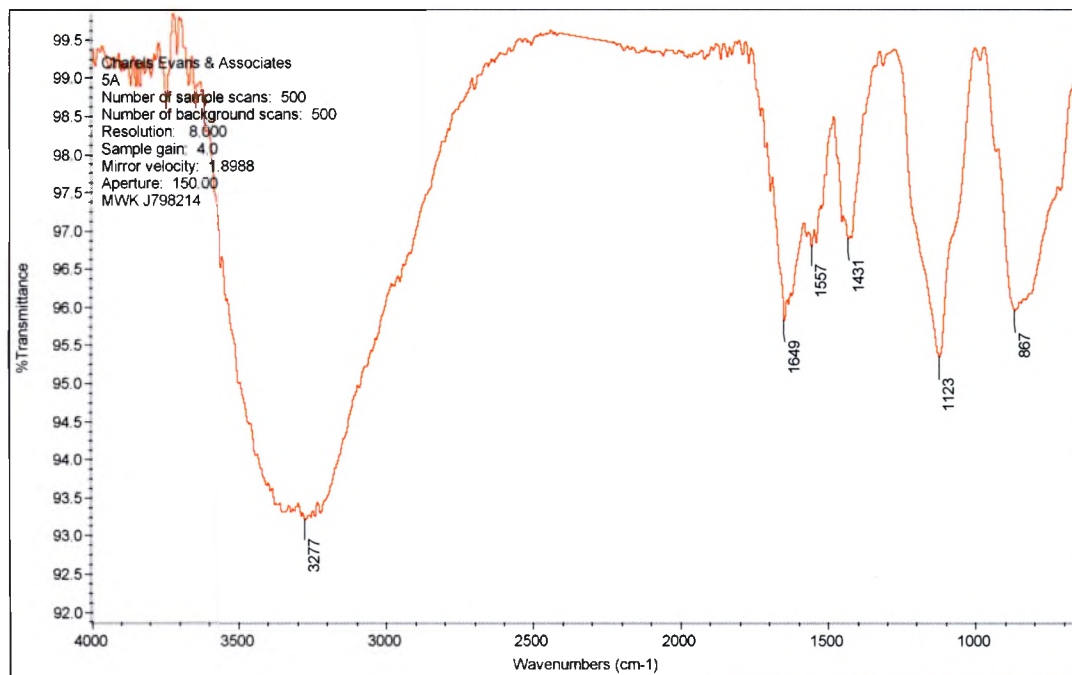


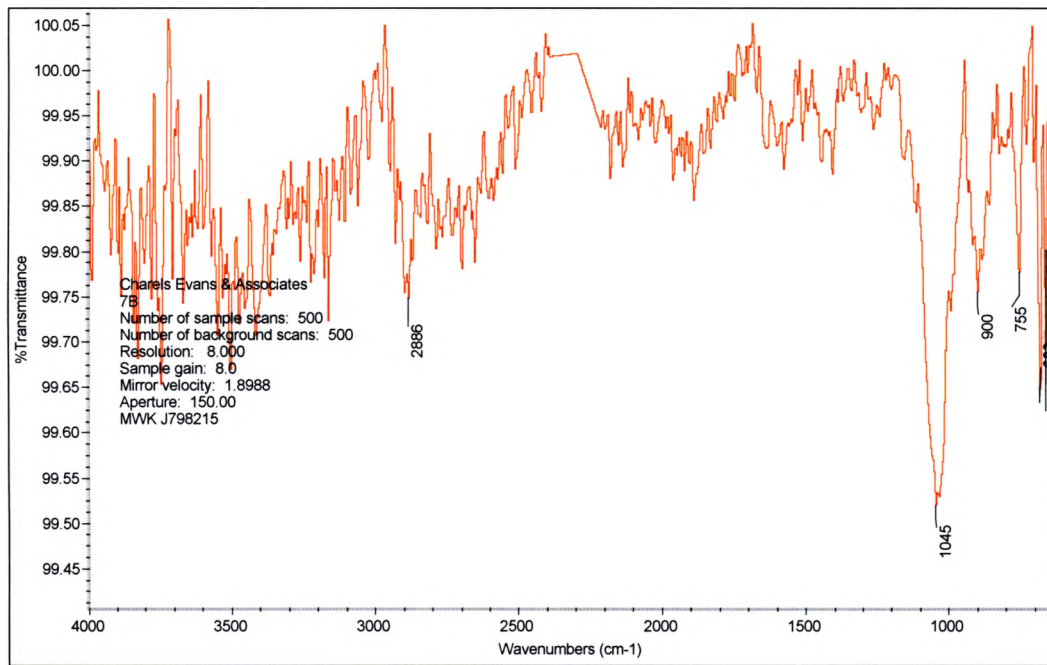
Figure 5.25 is the FTIR spectrum for specimen 3. It exhibited a broad peak centered at 3277 cm^{-1} . Its position and broadness suggest the presence of an organic acid. The peak centered at 1649 cm^{-1} is thought to be an amide signal, while the peak at 1123 cm^{-1} is possibly sulfate and sulfite. The characteristic PTFE bands visible in Specimens 1 and 2 are no longer present in Specimen 3.

Figure 5.25 FTIR spectrum of Specimen 3, subjected to 30-minutes of extreme wear conditions.



The FTIR spectrum for Specimen 4 is presented in Figure 5.26. The transmittance for the sample was very low, leading to a noisy spectrum. It reveals very little organic material remained after lubricant failure.

**Figure 5.26 FTIR spectrum of Specimen 4,
subjected to 60-minutes of extreme wear conditions.**



CHAPTER 6

CONCLUSIONS

6.1 Endurance Life and Corrosion Resistance

Advanced aerospace designs precipitated development of resin bonded lubricants in the 1950's. Since their inception, these products incorporated lead, antimony oxide, and hazardous solvents to meet MIL-L-23398 performance requirements. Consequently they fail to meet contemporary environmental and occupational exposure requirements. Restrictions and escalating costs of products developed prior to the Clean Air Act have created opportunities for conforming materials to displace those that do not comply. Research and development of novel, low VOC technologies can provide new substitutes that meet or exceed performance requirements.

Simultaneously meeting endurance life and corrosion resistance requirements with waterborne chemistry proved to be a technical challenge. Acceptable endurance life was achieved early using combinations of urethane resin and MoS₂ pigment. However, the lubricant rapidly induced corrosion on metal, and corrosion inhibiting additives were ineffectual. An iterative approach to formula modification identified silicone surfactants detrimental to corrosion protection. Further enhancements to product performance were achieved through optimized solids content and coalescent blends. A design of experiments graphically illustrated optimum blends through

minimal trials. Incorporation of PTFE enhanced endurance life of a corrosion resistant lubricant formulation, enabling it to meet development objectives.

Subjecting the lubricant to remaining performance tests of MIL-L-23398 confirmed its ability to meet all performance requirements.

6.2 Characterization

6.2.1 X-ray Photoelectron Spectroscopy

Analysis of the lubricant surface by XPS after various stages of wear showed distinct reactions occurred. The technique detected chemical reactions initiated by tribological processes. Significant shape changes of four survey spectra indicated dynamic chemistry on the lubricant surface.

Atomic concentrations of molybdenum and sulfur initially increased, but were almost absent after lubricant failure. MoS_2 was unaffected by reduced pressure wear on Specimen 2. However, XPS showed that the surface of Specimen 3 contained mixtures of MoS_2 and oxides of molybdenum after extreme pressure wear. Medium resolution spectra of Specimens 1 and 2 showed presence of sulfide, but a mixture of sulfide and sulfate on Specimen 3. This indicated that, under extreme pressure conditions, MoS_2 oxidized well below its air oxidization temperature of 400°C . These observations were consistent with Hsu's observations that forces associated with rubbing motions can induce spikes in temperature and pressure in the vicinity of asperities and lead to chemical reactions.²⁶ He has also suggested that reactions may be induced by rubbing of metal surfaces, exposing metal sites that may react with a lubricant directly or catalyze lubricant reactions. A third possibility is that disruption

of surface bonds by mechanical forces lead to charge-particle emission and formation of unsatisfied valencies. This in turn may stimulate chemical reactions.

Extreme pressure wear caused fluorine to rapidly decline over the series, indicating that PTFE may have stratified or bloomed to the lubricant surface. XPS studies by Pistillo of a worn cam shaft lobe lubricated with PTFE showed conversion of fluorine to a metal fluoride.³⁴ Binding energy shifts through the tested pin series of this study were consistent with Pistillo's observations and also showed formation of fluoride after wear. Absence of iron on Specimen 1 indicated that the coating thickness was over 100-angstroms. Detection of iron in Specimen 2 suggested rapid lubricant compaction from 5-microns to less than 100-angstroms.

6.2.2 Atomic Force Microscopy

AFM experiments showed rough surface topography of Specimen 1. The lubricant was not subjected to wear and therefore lubricating pigments were not burnished into parallel orientation. The mean roughness (R_a) and maximum height (R_{max}) of Specimen 1 reveal a homogeneous mixture of peaks and valleys. Evidence of solid PTFE on the surface by XPS, FTIR and the AFM results strongly suggest agglomerations of PTFE and urethane particles. Large decrease in Mean Roughness (R_a) between Specimens 1 and 2 showed effects of burnishing the lubricant at low pressure during break-in.

Increase of Mean Roughness and Maximum Height from Specimen 2 to Specimen 3, coupled with the XPS and FTIR data, suggest that MoS_2 , oxides of molybdenum ($MoOx$), sulfides (S^{2-}) and sulfates (SO_4^{2-}) predominate the surface of Specimen 3 as larger, rougher species than those on the surface of Specimen 2.

The dramatic decrease of Mean Roughness and Maximum Height observed for Specimen 4, coupled with the high iron content detected by XPS, suggest that the lubricant is almost completely removed. It appears that the steel surface beneath the coating is smooth, relative to the PTFE and MoS₂ particles. However, the relatively smooth steel surface provides little lubricating properties, unlike those observed for PTFE and MoS₂.

6.2.3 FTIR

The FT-IR spectrum obtained for Specimen 1 was consistent with the original materials of the lubricant. The ester peak at 1726 reciprocal centimeters (cm⁻¹) confirms the polyester backbone of the polyol used to prepare the urethane polymer. Absorption bands at 1226 and 1158 cm⁻¹ indicate the presence of PTFE that was also confirmed by XPS. Absence of absorption bands above 3000 cm⁻¹ indicated the aliphatic nature of the lubricant. The FTIR spectrum for Specimen 2 contained the same bands as Specimen 1, but also revealed formation of an organic acid with a broad band centered at 3437 cm⁻¹. Hsu observed formation of carboxylic acids when hydrocarbon lubricants were initially oxidized during extreme pressure wear.²⁶ It is believed that the polyurethane resin or glycol ether coalescent may have undergone a similar reaction to produce the acid observed in the spectrum.

An absorption band at 1123 cm⁻¹ in the FTIR spectrum of Specimen 3 appears to confirm the presence of sulfate and sulfite, as detected by XPS. The loss of bands associated with PTFE parallel the reduction of the compound observed by XPS. The FTIR spectrum for Specimen 4 is too noisy for definitive assignments; however, the greatly reduced transmittance suggests that very little organic material remained on

the surface. This result is consistent with the high percentage of iron detected by XPS and the surface topography resolved by AFM.

6.3 Future Work

The low VOC dry film lubricant was based upon MoS₂ as the lamellar solid capable of extreme pressure wear. Tungsten disulfide (WS₂) has also been used as a solid lubricant, and could enhance wear life of the product. A study could include direct replacement (or blends) of MoS₂ with WS₂.

Extreme pressure wear tests were performed using grit-blasted steel prior to lubricant application. It was not possible to obtain consistent phosphate pre-treatment and therefore was not used. However, the literature suggested that dry film lubricants have improved endurance life when applied to phosphate treated surfaces.¹² Therefore, comparative studies that include phosphate-treated specimens could help to determine optimum surface preparation for enhanced lubricant performance.

Spectroscopic analysis identified dynamic chemical reactions that occurred on the lubricant surface during wear. XPS and FTIR results were complimentary, but AFM results appeared independent. The literature suggests that AFM can be employed to characterize lubricants. However, it may be difficult for AFM to detect the same areas observed by XPS and FTIR due to greatly reduced scale of analysis. Ludema used a surface tracer to make larger scale surface roughness measurements, similar to AFM. That instrument analyzes greater surface area versus AFM. Its larger scale could better compliment XPS and FTIR results, through greater probability of observing the same region on the lubricant surface.

Scanning Electron Microscopy (SEM) experiments could also be considered to better characterize the lubricant after wear. Elemental analysis by SEM could compliment AFM and FTIR results

REFERENCES

1. ASTM D 2510 “Standard Test Method for Adhesion of Solid Film Lubricants.”
2. ASTM D 2511 “Standard Test Method for Thermal Shock Sensitivity of Solid Film Lubricants.”
3. ASTM D 2625 “Standard Test Method for Endurance (Wear) Life and Load Carrying Capacity of Solid Film Lubricants (Falex Pin and Vee Method).”
4. ASTM G15-83 “Standard Terminology Related to Corrosion and Corrosion Testing.
5. ASTM G99-95a “Standard Test Method for Wear Testing with a Pin On Disc Apparatus”.
6. Military Specification MIL-L-23398, Lubricant, Solid Film, Air-Cured, Corrosion Inhibiting, NATO Code Number S-749, 1985.
7. Military Specification MIL-PRF-46147, Performance Specification, Lubricant, Solid Film, Air Cured (Corrosion Inhibiting), 1994.
8. U.S. Provisional Patent Application, Serial Number 60/592,174, filed July 29, 2005.
9. Archer, R.S., Briggs, J.Z., Loeb, Jr., C.M., “Molybdenum Steels Irons Alloys”, Hudson Press, 1948.
10. Blank, W.J., Formulating Polyurethane Dispersions, Corporate Research Paper, King Industries, Norwalk, CT.
11. Boser, E.R., Tribology Data Handbook, CRC Press, Boca Raton, 1997.
12. Calhoun, S.F., Meade, F.S., Murphy, G.P., Young, R.L., “Factors Affecting the Performance of Resin Bonded Solid Film Lubricants”. *Lubrication Engineering*, Vol. 21, No. 3, March 1965.
13. Campbell, M., Hopkins, V., “Polyimide Bonded Solid Lubricants”, 22nd ASLE Annual Meeting Conference Paper, Toronto, Canada, May 1-4, 1967.
14. Carpick, R.W., Salmeron, M., “Scratching the Surface: Fundamental Investigations of Tribology with Atomic Force Microscopy”, Chem. Rev., 1997, 97, 1163-1194.

15. Chen, M., Zak, C., Cusack, T., Magee, W., Best of Both Worlds – Water-based acrylic/urethane hybrid system improves adhesion for food packaging, *Adhesives Age*, January/February 2003.
16. Coogan, R., Pollano, G., Advances In Water-borne Urethane Technology, *American Paint and Coatings Journal*, July 2, 1990.
17. DeLaat, F.G.A., Shelton, R.V., Kimzey, J.H., “Status of Lubricants for Manned Spacecraft”, *Lubrication. Engineering*, vol. 23, No. 4, April 1967.
18. Devine, M.J., Lamson, E.R, Cerini, J.P., McCartney, R.J., “Solids and Solid Lubrication”, *Lubrication Engineering*, January 1965.
19. Drisko, R.W., Jenkins, J.F., Corrosion and Coatings: An Introduction to Corrosion for Coatings Personnel, SSPC: The Society for Protective Coatings, SSPC 98-08.
20. Fiori, D.E., Ley, D.A., Quinn, R.J., Tertiary Isocyanates: The Choice for Waterborne Coatings, Corporate Research Paper, Cytec Industries, Inc., Stamford, CT, USA.
21. Fambri, L., Pegoretti, A., Gavazza, C., Penati, A., “Thermooxidative Stability of Different Polyurethanes Evaluated by Isothermal and Dynamic Methods, *Journal of Applied Polymer Science*, Vol. 81, 1216-1225, 2001.
22. Frisch, K.C., Klempner, D., “Advances in Urethane Science and Technology”, Editors, Vol. 10, pp. 121-162, 1987.
23. Ganster, O.R., Buechner, J., Dormish, J.F., Under the Microscope – Analyzing the Development and Properties of One-Component, PU-Dispersion Adhesives, *Adhesives Age*, August 2002.
24. Gestor, G., “Marine Corrosion, a thorough discussion of the many causes of metal corrosion”, *Good Old Boat*, September/October, 2005
25. Hare, C.H., “Protective Coatings, Fundamentals of Chemistry and Composition”, (Pittsburgh: The Society for Protective Coatings).
26. Jacoby, M., Molecular-Scale Wear and Tear, *Chemical and Engineering News*, Vol. 83, No. 43, p. 51, October 24, 2005
27. Hunter, J.S., "Applying Statistics to Solving Chemical Problems", *Chemtech*, 17, 167-169, 1987.

28. Kong, J., Park, K.T., "Molybdenum Disulfide Single Crystal (0002) Plane XPS Spectra", *Surface Science Spectra*, Vol. 7, No. 1, 2000.
29. Ludema, K., *Friction, Wear, Lubrication A Textbook in Tribology*, CRC Press Boca Raton, Florida, 1996.
30. Mayne, J.E.O., "Paints for the Protection of Steel – A review of Research into Their Modes of Action", *British Corrosion Journal*, p. 106, May 1970.
31. McNaughton, J.L., Mortimer, C.T., *Differential Scanning Calorimetry, IRS; Physical Chemistry Series 2, 1975, Volume 10*, Butterworths, London.
32. Moses, M., "Applying Solid Film Lubricants To Small Precision Timing Mechanisms With a Semi-Automated Process", *Conference proceedings, 21st ASLE Annual Meeting*, Pittsburgh, PA, May 2-5, 1966.
33. Petrie, E.M., *Handbook of Adhesives and Sealants*, (New York: McGraw-Hill, 2000).
34. Pistillo, W.R., *Engine Treatment Product Fleet Test and Engine Component Analysis*, SAE Fall Fuels and Lubricants Meeting and Exposition, San Francisco, CA, Document number 982440, October 1998.
35. Schneider, S., "Investigation to Remove Lead and Antimony from Solid Film Lubricants, TARDEC Technical Report No. 13800, U.S. Army TACOM, July 2001.
36. SSPC Staff Article, "Cost of corrosion: \$300 billion a year", *Materials Performance*, Vol. 34, No. 5, June 1995.
37. Tramontano, V.J., Thomas, M.E., Coughlin, R.D., *Synthesis and Coating Properties of Novel Waterborne Polyurethane Dispersions*, Corporate Research Paper, King Industries, Norwalk, CT, USA.
38. U.S. Patent #5,856,404, *Backbedding Sealant Composition*, Assignee Schnee-Morehead, January, 1999.
39. Voynick, S.M., "Climax, The History of Colorado's Climax Molybdenum Mine", Mountain Press Publishing Company, Missoula, Montana, 1996.
40. Walker, G., Gustafson, J.H., "Airframe and Accessory Lubricants", *SAE National Aerospace Engineering and Manufacturing Meeting*, Los Angeles, CA, Oct. 8-12, 1962.
41. Watts, J.F., Wolstenholme, J., *An Introduction to Surface Analysis by XPS and AES*, Wiley, New York, 2003.

42. Williams, J.A., *Engineering Tribology*, Oxford University Press, New York, 1994.
43. Wills, B.A., "Mineral Processing Technology, An Introduction to the Practical Aspects of Ore Treatment and Mineral Recovery", Pergamon Press, Oxford, 1979.
44. Wolfe, G.F., "Effect of Surface Coatings on the Load Carrying Capacity of Steel", *Lubrication Engineering*, January 1963.
45. Handbook of X-ray Photoelectron Spectroscopy, Physical Electronics, Inc. © 1995.
46. NIST XPS Database, version 3.0

VITA

Aureliano Perez, Jr. was born in Port Huron, Michigan on February 8, 1967, the son of Aureliano and Theresa Perez. He started his undergraduate studies at Macomb County Community College, and received his Bachelor of Science degree in Chemistry from Wayne State University in December, 1991. Aureliano moved to Austin, Texas in 1998, and entered the Graduate School at Texas State University – San Marcos in August, 2003.

Permanent Address: 12616 Grimes Ranch Court
Austin, Texas 78732

This thesis was typed by Aureliano Perez, Jr.